

# FREQUENCY SHIFTING FOR SOLITONS BASED ON TRANSFORMATIONS IN THE FOURIER DOMAIN AND APPLICATIONS

TOAN T. HUYNH AND QUAN M. NGUYEN

**ABSTRACT.** We develop the theoretical procedures for shifting the frequency of a single soliton and of a sequence of solitons of the cubic nonlinear Schrödinger (NLS) equation. The procedures are based on simple transformations of the soliton pattern in the Fourier domain and on the shape-preserving property of solitons. We verify these theoretical frequency shifting procedures by numerical simulations with the NLS equation using the split-step Fourier method. We demonstrate the use of the frequency shifting procedures for two important applications: (1) stabilization of the propagation of solitons in waveguides with frequency dependent linear gain-loss; (2) induction of repeated soliton collisions in waveguides with weak cubic loss. The results of our extensively numerical simulations with the cubic NLS equation are in very good agreement with the theoretical predictions.

*Keywords:* Soliton, nonlinear Schrödinger (NLS) equation, frequency shift, Fourier transform.

*Mathematics Subject Classification (2010):* 35Q51, 35Q55, 34A34, 78A10.

## 1. INTRODUCTION

Solitons are stable shape preserving traveling-wave solutions of a class of nonlinear partial differential equations such as the NLS equation, the Ginzburg-Landau equation, the sine-Gordon equation, and the Korteweg-de Vries equation [1, 2, 3]. In nonlinear dispersive media, the perfect balance between nonlinearity and dispersion forms solitons. Solitons appear in a wide range of fields, including hydrodynamics [4], condensed matter physics [5], optics [6, 7, 8], and plasma physics [9]. One of the most fundamental properties of solitons is their shape-preserving property in a soliton collision, that is, a soliton collision is elastic [10, 11, 12]. In 1973, Hasegawa and Tappert showed the existence of solitons in optical fibers, which can be described by the cubic NLS equation [13]. Due to the integrability of the NLS equation and the stability of optical solitons, they are ideal candidates for information transmission and processing in broadband waveguide systems [6, 8]. In the optical fiber transmission technology, temporal solitons of the NLS equation can be used as bits of information [6, 8]. This has lead to the explosion of high-speed communication technologies based on solitons transmission in the last three decades.

A soliton of the cubic NLS equation (NLS soliton) is characterized by four parameters: its amplitude ( $\eta$ ), phase ( $\alpha$ ), position ( $y$ ), and frequency ( $\beta$ ). The group velocity  $v_g$  of a soliton is double its central frequency, i.e.,  $v_g = 2\beta$ . In broadband waveguide systems, many sequences of solitons can propagate through the same waveguide. The solitons in each sequence (each “frequency channel”) propagate with the same group velocity, but the group velocity differs for solitons from different sequences. The frequency shift process is a physical or artificial process that changes the frequency of a soliton (or, of a sequence of solitons), and so its velocity and, as a consequence, changes the bit rate in transmission. In this process, the frequency of solitons is shifted to a new frequency while other parameters of the solitons are kept intact. The soliton frequency shifting has been widely studied recently for its important applications in soliton-based transmissions and signal processing. More specifically, in fiber-optics technology, a few techniques of frequency shifting have been developed such as methods of wavelength conversion [14] and of coherent detection [15] in which one can extract any phase, amplitude, and frequency carried by a transmitted electric

field. A physical process which affects the frequency of optical solitons is the Raman self frequency shift, which is a continuous downshift of the soliton frequency due to energy transferring from high-frequency components of the soliton to lower ones [6, 16]. There have been several previous studies related to the soliton frequency shift, especially the self frequency shift, for example, see [16, 17, 18, 19, 20]. The implementation of frequency shifting, in particular, for a sequence of solitons, is challenging since it is difficult to shift only the frequency by an arbitrary large value while keeping other parameters unchanged. As shown in section 2.2.2 of the current paper, a “naive” frequency shifting procedure for a sequence of solitons might lead to a change of the phase of new pulses. Recently, in [20], the authors found a way to introduce a large frequency shift to solitons along a waveguide using the delayed Raman response or guiding filters with a varying central frequency. However, this method is also limited since it shifts the frequency only of the soliton and not of the accompanying radiation. In addition, the soliton’s frequency shift developed in [20] might not be applied for shifting an arbitrary frequency at a certain propagation distance. So far, to the best of our knowledge, a complete mathematical procedure for frequency shifting of any given frequency at a given propagation distance is still lacking.

In the current paper, we address this important and challenging task. We develop the theoretical procedures for shifting the frequency of a single NLS soliton and of a sequence of NLS solitons, and verify them by simulations. The procedures of frequency shifting are based on simple transformations of the Fourier transform (FT) of the wave field in the Fourier domain (or the frequency domain). In particular, we develop the *decomposition method* to perform frequency shifting for a sequence of solitons. Furthermore, we also present two major applications for the use of soliton frequency shifting. We apply frequency shifting procedures to: (1) stabilize the propagation of solitons in waveguides with frequency dependent linear gain-loss; (2) enable repeated two-soliton collisions in the presence of weak cubic loss. In the first application, we show that the dynamics of the soliton amplitude in waveguides with frequency dependent linear gain-loss can be described by an ordinary differential equation (ODE). We then use this ODE to study the robust propagation of a single soliton and a sequence of solitons experiencing frequency dependent linear gain-loss in multiple periodic frequency shifting. The soliton dynamics studied in work can be used for controlling and switching soliton sequences in broadband waveguides. Furthermore, in experiments and simulations, it is often difficult to measure a very small quantity such as a collision-induced amplitude shift due to the effect of weak perturbation. In the second application, we suggest a solution for this problem by the use of the frequency shifting to repeat two-soliton collisions in the presence of weak cubic loss. As a result, we are able to measure the theoretical prediction for the accumulative amplitude shift from several repeated collisions, which is a much larger value.

The use of frequency dependent linear gain-loss for the transmission stability of NLS solitons was recently studied in several previous papers such as [20, 21, 22, 23]. In these papers, it is shown that the use of frequency dependent linear gain-loss can suppress radiative effects and stabilize multi-sequence soliton propagation at long distances. The main factor for the stabilization propagation is due to the fact that the use of frequency dependent linear gain-loss is efficient in suppressing the resonant part of the emitted radiation [20]. Furthermore, the waveguide’s cubic loss can be a result of two-photon absorption (TPA) or gain and loss saturation in a silicon waveguide. TPA recently received considerable attention due to the importance of TPA in silicon nanowaveguides, which are expected to play a crucial role in optical processing applications in optoelectronic devices, including pulse switching and compression, wavelength conversion, regeneration, etc [24, 25, 26, 27]. Soliton propagation of the NLS equation with weak cubic loss has also been investigated in many previous papers such as [22, 25, 26, 27, 28]. It has been shown that the presence of weak cubic loss can affect soliton dynamics and, in particular, lead to a downshift of the amplitude and frequency of solitons in a single two-soliton collision. The analytic expressions for the amplitude and frequency shift in a single two-soliton collision in the presence of weak cubic loss were found in [25].

The rest of the paper is organized as follows. In section 2, we develop the frequency shifting procedures for a single NLS soliton and a sequence of NLS solitons. In section 3, we theoretically analyze applications of frequency shifting for a single soliton and a sequence of solitons as follows: (1) stabilizing soliton propagation in waveguides with frequency dependent linear gain-loss; (2) enabling repeated two-soliton collisions in the presence of weak cubic loss and then measure the theoretical prediction for the accumulative amplitude shift. In section 4, we verify the theoretical results presented in section 2 and section 3 by numerical simulations with the cubic NLS equation. Section 5 is reserved for conclusions. In Appendix A and B, we present the implementations of frequency shifting procedures for a single soliton and a sequence of solitons in numerical simulations. In Appendix C, we describe the split-step Fourier method for numerical simulations with the NLS equation.

## 2. THE THEORETICAL PROCEDURES FOR FREQUENCY SHIFTING

**2.1. Model, solitons and their Fourier transforms.** In this section, we describe the NLS solitons and their Fourier transforms. The propagation of solitons through a nonlinear optical waveguide can be described by the unperturbed cubic NLS equation [1, 2, 6, 12]:

$$i\partial_z\psi + \partial_t^2\psi + 2|\psi|^2\psi = 0, \quad (2.1)$$

where  $\psi$  is proportional to the envelope of the electric field,  $z$  is the normalized propagation distance, and  $t$  is the time [29]. The second term of Eq. (2.1) describes the effects of temporal second-order dispersion while the third term describes the effects of Kerr nonlinearity. Equation (2.1) has the fundamental soliton solution which is given by [1, 2, 6, 30]:

$$\psi_0(t, z) = \eta \frac{\exp(i\chi)}{\cosh(x)}, \quad (2.2)$$

where  $x = \eta(t - y_0 - 2\beta z)$ ,  $\chi = \alpha + \beta(t - y_0) + (\eta^2 - \beta^2)z$ , and  $\eta$ ,  $\beta$ ,  $y_0$ , and  $\alpha$  are the soliton amplitude, frequency, initial position, and phase, respectively.

First, we calculate the Fourier transform of a single soliton. We consider the initial condition in form of

$$\psi_1(t, 0) = \eta(0) \frac{\exp\{i[\alpha(0) + \beta(0)(t - y(0))]\}}{\cosh\{\eta(0)[t - y(0)]\}}, \quad (2.3)$$

where  $\eta(0)$ ,  $\beta(0)$ ,  $y(0)$ , and  $\alpha(0)$  are the initial soliton's amplitude, frequency, position, and phase, respectively. In a typical optical waveguide system, solitons propagate in the presence of additional weak physical perturbations, such as linear or nonlinear loss, Raman scattering, etc. [6]. In the current work, we assume that the effects of these perturbation processes on soliton propagation are weak. Under this assumption, we can employ the standard adiabatic perturbation theory for the NLS soliton and write the total electric field at a distance  $z$  as:  $\psi(t, z) = \psi_{s1}(t, z) + v_{r1}(t, z)$ , where  $\psi_{s1}(t, z)$  is the soliton part, and  $v_{r1}(t, z)$  is the very small radiation part [31]. The soliton part  $\psi_{s1}(t, z)$  is expressed as

$$\psi_{s1}(t, z) = \eta(z) \frac{\exp\{i[\beta(z)(t - y(z)) + \theta(z)]\}}{\cosh\{\eta(z)[t - y(z)]\}}, \quad (2.4)$$

where  $\eta(z)$ ,  $\beta(z)$ ,  $y(z)$ , and  $\theta(z)$  are the  $z$ -dependent soliton's amplitude, frequency, position, and overall phase, respectively. The FT of  $\psi_{s1}(t, z)$  with respect to  $t$  is defined by

$$\hat{\psi}_{s1}(\omega, z) = \frac{1}{(2\pi)^{1/2}} \int_{-\infty}^{\infty} \psi_{s1}(t, z) e^{-i\omega t} dt, \quad (2.5)$$

where  $\omega$  is frequency. Thus,

$$\hat{\psi}_{s1}(\omega, z) = \frac{\eta(z)}{(2\pi)^{1/2}} e^{i\theta(z)} \int_{-\infty}^{\infty} \frac{e^{i\beta(z)[t-y(z)]} e^{-i\omega t}}{\cosh\{\eta(z)[t-y(z)]\}} dt. \quad (2.6)$$

By the Residue theorem, one can obtain  $\int_{-\infty}^{\infty} \frac{e^{-ibx}}{\cosh(ax)} dx = \frac{\pi/a}{\cosh[\pi b/(2a)]}$ , where  $a$  and  $b$  are constants,  $a > 0$  and  $b \in \mathbb{R}$ . Therefore, Eq. (2.6) yields the pattern of a single soliton in the frequency domain:

$$\hat{\psi}_{s1}(\omega, z) = \left(\frac{\pi}{2}\right)^{1/2} \frac{\exp[i\theta(z) - i\omega y(z)]}{\cosh\{\pi[\omega - \beta(z)]/[2\eta(z)]\}}. \quad (2.7)$$

Second, we turn to calculate the FT of a sequence of solitons. We assume that the envelope of the electric field at the waveguide's entrance consists of  $2J + 1$  solitons with equal initial amplitudes, frequencies, and phases. This sequence of solitons can be used in a finite waveguide link or in a closed waveguide loop. Thus, the initial soliton sequence  $\psi_{sq}(t, 0)$  is given by

$$\psi_{sq}(t, 0) = \sum_{k=-J}^J \frac{\eta(0) \exp\{i[\alpha(0) + \beta(0)(t - y(0) - kT)]\}}{\cosh[\eta(0)(t - y(0) - kT)]}, \quad (2.8)$$

where  $\eta(0)$ ,  $\beta(0)$ , and  $\alpha(0)$  are the common initial amplitude, frequency, and phase,  $y(0)$  is the initial position of the central soliton, and  $T$  is the temporal separation between adjacent solitons, i.e., the time-slot width. Assuming the soliton sequence propagates in the presence of weak physical perturbations, the total electric field at a propagation distance  $z$  can be written as:  $\psi(t, z) = \psi_{sq}(t, z) + v_{rq}(t, z)$ , where  $\psi_{sq}(t, z)$  is the soliton sequence and  $v_{rq}(t, z)$  is the very small radiation part [31]. The soliton sequence  $\psi_{sq}(t, z)$  can be expressed as

$$\psi_{sq}(t, z) = \eta(z) e^{i\theta(z)} \sum_{k=-J}^J \frac{\exp\{i\beta(z)[t - y(z) - kT]\}}{\cosh\{\eta(z)[t - y(z) - kT]\}}, \quad (2.9)$$

where  $\eta(z)$ ,  $\beta(z)$ ,  $y(z)$ , and  $\theta(z)$  are the common amplitude, frequency, overall position shift, and overall phase of solitons at the distance  $z$ , respectively. The FT of  $\psi_{sq}(t, z)$  with respect to time is given by

$$\hat{\psi}_{sq}(\omega, z) = \left(\frac{\pi}{2}\right)^{1/2} \frac{\exp[i\theta(z) - i\omega y(z)]}{\cosh\{\pi[\omega - \beta(z)]/[2\eta(z)]\}} \sum_{k=-J}^J e^{-ikT\omega}. \quad (2.10)$$

This can be written as

$$\hat{\psi}_{sq}(\omega, z) = V(\omega, z) W(\omega) e^{iU(\omega, z)}, \quad (2.11)$$

where

$$V(\omega, z) = \left(\frac{\pi}{2}\right)^{1/2} \operatorname{sech}\left\{\frac{\pi[\omega - \beta(z)]}{2\eta(z)}\right\}, \quad (2.12)$$

$$W(\omega) = \sum_{k=-J}^J e^{-ikT\omega} = 1 + 2 \sum_{k=1}^J \cos(kT\omega), \quad (2.13)$$

and

$$U(\omega, z) = \theta(z) - \omega y(z). \quad (2.14)$$

The function  $V(\omega, z)$  describes the spectral shape of a single soliton in the frequency domain,  $W(\omega)$  is related to the solitons' positions relative to one another, while  $U(\omega, z)$  is the overall common phase. Figure 1 illustrates a typical example for a sequence of solitons  $|\psi_{sq}(t, z)|$ , its FT  $|\hat{\psi}_{sq}(\omega, z)|$ ,

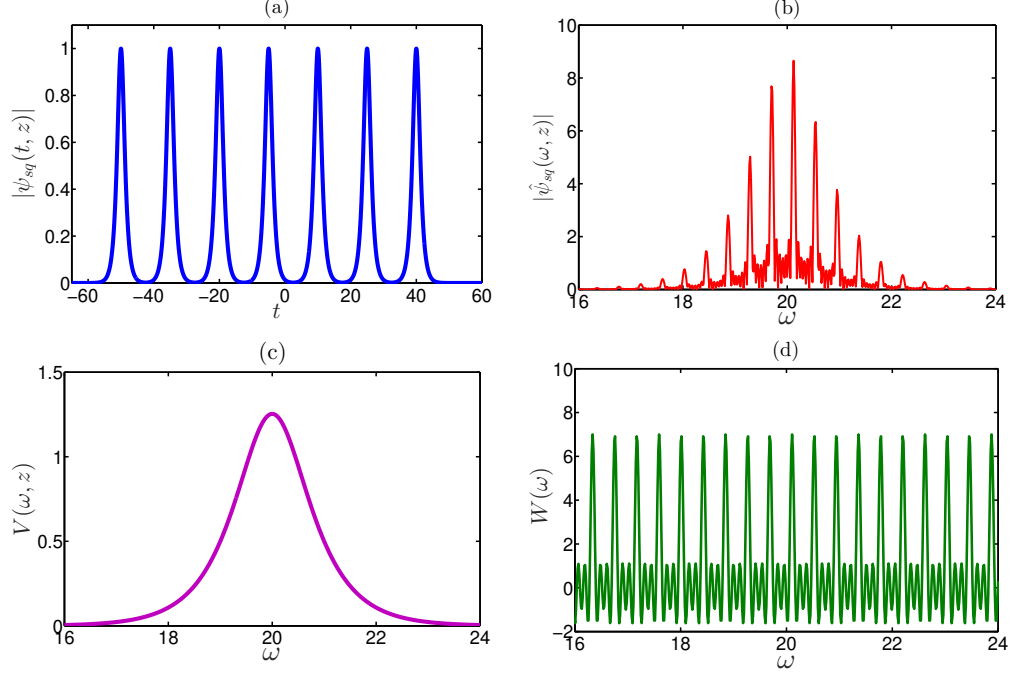


FIGURE 1. (Color online) The soliton pattern  $|\psi_{sq}(t, z)|$ , its FT pattern  $|\hat{\psi}_{sq}(\omega, z)|$ , and the functions  $V(\omega, z)$  and  $W(\omega)$ , given by Eqs. (2.9)-(2.13) with  $J = 3$ ,  $\eta(z) = 1$ ,  $\beta(z) = 20$ ,  $y(z) = -5$ , and  $T = 15$ . (a) The solid blue curve represents  $|\psi_{sq}(t, z)|$  obtained by Eq. (2.9). (b) The solid red curve represents the FT  $|\hat{\psi}_{sq}(\omega, z)|$  of pulse pattern in (a). (c) The solid purple curve represents  $V(\omega, z)$  obtained by Eq. (2.12). (d) The solid green curve represents  $W(\omega)$  obtained by Eq. (2.13).

$V(\omega, z)$ , and  $W(\omega)$ . It is seen that  $V(\omega, z)$  is related to an envelope function for  $|\hat{\psi}_{sq}(\omega, z)|$ , while  $W(\omega)$  corresponds to oscillations of the pulse pattern  $|\hat{\psi}_{sq}(\omega, z)|$  inside  $V(\omega, z)$ .

## 2.2. The frequency shifting procedures.

**2.2.1. Frequency shifting for a single soliton.** The frequency shifting procedure for a single soliton is simply based on shifting the pulse pattern in the frequency domain by a given value  $\Delta\beta$ . If the FT of a soliton before performing the frequency shifting is centered at  $\beta(z)$ , then it will be centered at the new frequency  $\beta_n(z) = \beta(z) + \Delta\beta$  after employing the frequency shifting. Formally, frequency shifting is implemented by employing the transformation  $\omega \rightarrow \omega - \Delta\beta$  on the Fourier domain. From Eq. (2.7), we obtain the FT of the soliton after performing the frequency shifting:

$$\hat{\psi}_{s1,n}(\omega, z) = \left(\frac{\pi}{2}\right)^{1/2} \frac{\exp[i\theta_n(z) - i\omega y(z)]}{\cosh\{\pi[\omega - \beta_n(z)]/[2\eta(z)]\}}, \quad (2.15)$$

where  $\theta_n(z) = \theta(z) + \Delta\beta y(z)$  is the *new* overall phase, the sub-index  $n$  denotes the *new* parameter of the pulse pattern after employing the frequency shifting. Taking the inverse FT of  $\hat{\psi}_{s1,n}$  with respect to  $\omega$ , we obtain the *new* (frequency shifted) soliton:

$$\psi_{s1,n}(t, z) = \eta(z) \frac{\exp\{i[\beta_n(z)(t - y(z)) + \theta_n(z)]\}}{\cosh\{\eta(z)[t - y(z)]\}}. \quad (2.16)$$

Compare Eq. (2.16) with Eq. (2.4), we conclude that after performing the frequency shifting we obtain the soliton with the new frequency  $\beta_n(z) = \beta(z) + \Delta\beta$ .

2.2.2. *Frequency shifting for a sequence of solitons.* We now present the frequency shifting procedure for a sequence of solitons propagating through a nonlinear optical waveguide. We assume that the soliton sequence propagates in the presence of weak physical perturbations. The soliton sequence is given by Eq. (2.9) and its FT is given by Eq. (2.11). We emphasize that the current frequency shifting procedure can be used in the following setups: (i) transmission through a finite-length optical waveguide link; (ii) propagation in a closed optical waveguide loop. The frequency shift method for a sequence of solitons is more complicated than for a single soliton. Before describing the decomposition procedure in the *procedure III*, we present and discuss the first two problematic procedures:

*Procedure I - a “naive” frequency shifting procedure.* First, we show that a frequency shifting procedure, which is based on a “naive” attempt to extend the procedure used for a single soliton to a sequence of solitons, is generally not applicable. In this “naive” procedure, one simply performs the transformation  $\omega \rightarrow \omega - \Delta\beta$  of the FT of the soliton sequence in the frequency domain. Indeed, by performing this transformation to the FT of a soliton sequence, which is given by Eq. (2.10), we arrive at the following expression for the FT of the soliton sequence after employing the frequency shifting:

$$\hat{\psi}_{sq,n}(\omega, z) = \left(\frac{\pi}{2}\right)^{1/2} \frac{\exp[i\theta_n(z) - i\omega y(z)]}{\cosh\{\pi[\omega - \beta_n(z)]/[2\eta(z)]\}} \sum_{k=-J}^J e^{-ikT\omega} e^{ikT\Delta\beta}, \quad (2.17)$$

where  $\theta_n(z) = \theta(z) + \Delta\beta y(z)$  is the *new* overall phase. Taking the inverse FT of  $\hat{\psi}_{sq,n}$  with respect to  $\omega$ , we obtain the new sequence of pulses:

$$\psi_{sq,n}(t, z) = \eta(z) e^{i\theta_n(z)} \sum_{k=-J}^J \frac{\exp\{i\beta_n(z)[t - y(z) - kT] + ikT\Delta\beta\}}{\cosh\{\eta(z)[t - y(z) - kT]\}}. \quad (2.18)$$

Compare Eq. (2.18) with Eq. (2.9), we see that the new pulse sequence does not have the form expected for a sequence of solitons due to the multiplicative phase factor  $\exp(ikT\Delta\beta)$  in Eq. (2.18). Note that if  $\Delta\beta = 2m\pi/T$ , where  $m \in \mathbb{Z}$ , then  $\exp(ikT\Delta\beta) = 1$  for  $-J \leq k \leq J$ . As a result, in this specific case, Eq. (2.18) has the same form with Eq. (2.9). Therefore, the *procedure I* is only applicable when  $\Delta\beta$  is an integer multiple of  $2\pi/T$ . This problem will be fixed in the decomposition procedure as described in the *procedure III*.

*Procedure II - the frequency shifting of  $V(\omega, z)$  and  $U(\omega, z)$ .* We present another theoretical approach to perform the frequency shift for a sequence of solitons. A promising theoretical procedure for employing the frequency shifting by a value  $\Delta\beta$  for a sequence of solitons in form of Eq. (2.9), which is called the “shifting envelope” procedure, is described as follows. First, we employ the frequency shift by the transformation  $\omega \rightarrow \omega - \Delta\beta$  for  $V(\omega, z)$  and  $U(\omega, z)$  in Eq. (2.11):

$$U_n(\omega, z) = U(\omega - \Delta\beta, z), \quad V_n(\omega, z) = V(\omega - \Delta\beta, z). \quad (2.19)$$

Second, we define the FT of the new pulse pattern after employing the frequency shifting:

$$\hat{\psi}_{sq,n}(\omega, z) = V_n(\omega, z) W(\omega) e^{iU_n(\omega, z)}. \quad (2.20)$$

Thus, in Eq. (2.20), the frequency shift is performed in the normalized “envelope function”  $V(\omega, z)$  and the phase  $U(\omega, z)$ , while  $W(\omega)$  is kept to be fixed during the transformations. Eq. (2.20) can be written as

$$\hat{\psi}_{sq,n}(\omega, z) = \left(\frac{\pi}{2}\right)^{1/2} \frac{\exp[i\theta_n(z) - i\omega y(z)]}{\cosh\{\pi[\omega - \beta_n(z)]/[2\eta(z)]\}} \sum_{k=-J}^J e^{-ikT\omega}. \quad (2.21)$$



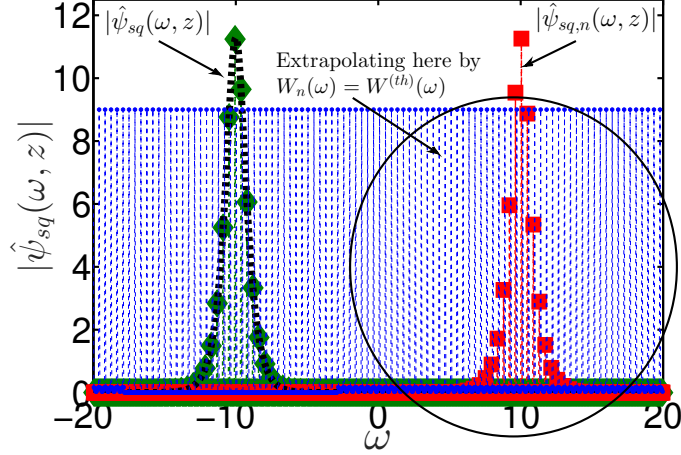


FIGURE 2. (Color online) The frequency shifting for a sequence of solitons by *procedure II* with  $\Delta\beta = 20$  at  $z = 5$ . The black dashed-dotted curve represents  $\hat{V}^{(num)}(\omega, z)$  as in appendix B. The blue circles represent  $|W^{(num)}(\omega)|$  measured by Eq. (2.72). The green diamonds represent  $|\hat{\psi}_{sq}(\omega, z)|$  measured by the numerical simulation with Eq. (2.1) and the red squares represent the new pattern of  $|\hat{\psi}_{sq,n}(\omega, z)|$  as obtained by Eq. (2.74).

Third, taking the inverse FT to Eq. (2.21), we then obtain

$$\psi_{sq,n}(t, z) = \eta(z) e^{i\theta_n(z)} \sum_{k=-J}^J \frac{\exp\{i\beta_n(z) [t - y(z) - kT]\}}{\cosh\{\eta(z) [t - y(z) - kT]\}}. \quad (2.22)$$

Equation (2.22) has the required form of the new theory prediction for a sequence of solitons, it preserves the relative phase between solitons.

*Shortcomings of the procedure II.* In theory, the *procedure II* is applicable since Eq. (2.22) has the same form with Eq. (2.9). However, it is important to emphasize the important shortcomings of the second frequency shifting procedure in numerical implementations. To explain this, we note that the pulse pattern in the frequency domain after performing the frequency shifting  $\hat{\psi}_{sq,n}^{(num)}(\omega, z)$  must be centered at the *new* numerical frequency value  $\beta_n^{(num)}(z)$ , where  $\beta_n^{(num)}(z) = \beta^{(num)}(z) + \Delta\beta^{(num)}$ . Therefore, the high accuracy of the numerical measurements and implementations for  $\beta^{(num)}(z)$ ,  $\Delta\beta^{(num)}$ ,  $V_n^{(num)}(\omega, z)$ ,  $W^{(num)}(\omega)$ , and  $U_n^{(num)}(\omega, z)$  in the neighborhood of  $\beta_n^{(num)}(z)$  is extremely important. These values can be determined by the procedures described as in Appendix B. As analyzing in Appendix B,  $W^{(num)}(\omega)$  are determined by the extrapolations for  $\omega < \beta^{(num)}(z) - L/2$  and  $\omega > \beta^{(num)}(z) + L/2$ , where  $15 \leq L \leq 40$  as mentioned in this Appendix. Consequently, if  $|\Delta\beta^{(num)}|$  is large,  $|\Delta\beta^{(num)}| \simeq L/2$  or  $|\Delta\beta^{(num)}| > L/2$ , then the numerical data points used for calculating  $W^{(num)}(\omega)$  of the main body of  $\hat{\psi}_{sq,n}^{(num)}(\omega, z)$ , i.e., in the neighborhood of  $\beta_n^{(num)}(z)$ , are obtained by extrapolations. These extrapolations in the main body of the new soliton pattern might lead to inaccuracies for calculating  $\hat{\psi}_{sq,n}^{(num)}(\omega, z)$  and, especially, change the physical effect of the soliton sequence, and as a result, to the breakdown of the frequency shifting procedure. Therefore, the *procedure II* can only be accurately implemented for a small value of the frequency shift:  $|\Delta\beta| \ll L/2$ .

In Fig. 2, we illustrate the important shortcomings of the *procedure II*. We perform the frequency shifting by Eq. (2.19) and Eq. (2.20) for a sequence of nine solitons. This figure depicts the

soliton patterns in the frequency domain before and after shifting the frequency,  $|\hat{\psi}_{sq}(\omega, z)|$  and  $|\hat{\psi}_{sq,n}(\omega, z)|$ , at the propagation distance  $z_s = 5$ . The parameters are  $\Delta\beta = 20$ ,  $L = 15$ ,  $\eta(0) = 1$ ,  $\beta(0) = -10$ ,  $y(0) = -5$ ,  $\alpha(0) = 0$ ,  $t_{\max} = 67.5$ ,  $t_{\min} = -t_{\max}$ ,  $T = 15$ , and  $J = 4$ . The numerical shifting value is  $\Delta\beta^{(num)} = 20.0131$  and the number of grid points shifted on the frequency domain is  $n_{shift} = 430$ . The numerical measurements for the frequency before and after performing the frequency shifting are  $\beta^{(num)}(z = 5) = -10$  and  $\beta_n^{(num)}(z = 5) = 10.0131$ , respectively. As can be seen, in the circled region in Fig. 2, we need to extrapolate  $W(\omega)$  by using the theoretical prediction  $W^{(th)}(\omega)$  for  $\omega > \beta^{(num)}(z) + L/2 = -2.5$  (see appendix B). As a result, extrapolated values of  $W(\omega)$  are used for calculating  $\hat{\psi}_{sq,n}^{(num)}(\omega, z)$  in the main body of  $\hat{\psi}_{sq,n}^{(num)}(\omega, z)$ .

*Procedure III - the decomposition procedure.* This method can completely fix the mentioned impairments of both previous procedures. This new method, which is called the decomposition method, is based on the following key ideas: (1) The “naive” procedure I works perfectly for a frequency shift value of  $\Delta\beta = 2m\pi/T$ ,  $m \in \mathbb{Z}$ . (2) The impairment of the “shifting envelope” procedure in the procedure II can be fixed by shifting a small frequency value  $\Delta\beta$ :  $|\Delta\beta| \ll L/2$ . The theoretical procedure of the decomposition method can be summarized as follows:

- (1) Decompose  $\Delta\beta = \Delta\beta_1 + \Delta\beta_2$ , where  $\Delta\beta_1 = 2m\pi/T$ ,  $m \in \mathbb{Z}$ , and  $-2\pi/T < \Delta\beta_2 < 2\pi/T$ .
- (2) Define  $\hat{\psi}_{sq,n1}(\omega, z) = \hat{\psi}_{sq}(\omega - \Delta\beta_1, z)$  by the “naive” method as the *procedure I*.
- (3) Employ the frequency shift by  $\Delta\beta_2$  for  $\hat{\psi}_{sq,n1}(\omega, z)$  by using the *procedure II*. That is,  $\hat{\psi}_{sq,n}(\omega, z) = V_n(\omega, z)W(\omega)e^{iU_n(\omega, z)}$  as in Eqs. (2.19)-(2.20).
- (4) Define  $\psi_{sq,n}(t, z) = \mathcal{F}^{-1}(\hat{\psi}_{sq,n}(\omega, z))$ , where  $\mathcal{F}^{-1}$  is the inverse FT.

To illustrate the decomposition method, we present the frequency shifting procedure for a soliton sequence propagating periodically in a waveguide loop. Figure 3 presents the frequency shifting procedure for a sequence of nine solitons at the propagation distance  $z_s = 5$  based on the decomposition method. The parameters are the same as parameters used for Fig. 2 with the *procedure II*:  $\Delta\beta = 20$ ,  $L = 15$ ,  $\eta(0) = 1$ ,  $\beta(0) = -10$ ,  $y(0) = -5$ ,  $\alpha(0) = 0$ ,  $t_{\max} = 67.5$ ,  $t_{\min} = -t_{\max}$ ,  $T = 15$ , and  $J = 4$ . We then measure  $\Delta\omega = 0.0465$  and  $\Delta\beta^{(num)} = 20.0131$  ( $n_{shift} = 430$ ) that consists  $\Delta\beta_1 = 94\pi/T = 19.6873$  ( $n_{shift} = 423$ ) and  $\Delta\beta_2 = 0.3258$  ( $n_{shift} = 7$ ). The numerical measurements for the frequency before and after performing the frequency shifting are  $\beta^{(num)}(z = 5) = -10$  and  $\beta_n^{(num)}(z = 5) = 10.0131$ , respectively. Figure 3(a) illustrates the first step of the procedure with shifting the frequency by  $\Delta\beta_1$ , that is, we obtain  $\hat{\psi}_{sq,n1}^{(num)}(\omega, z)$  from Eq. (2.75). Figure 3(b) represents the second step of the procedure with shifting the frequency by  $\Delta\beta_2$ . Figure 3(c) shows the comparison of the oscillation function  $|W^{(num)}(\omega)|$  measured by Eq. (2.72) and its theoretical prediction  $|W^{(th)}(\omega)|$ . Figure 3(d) shows the pulse patterns  $|\psi_{sq}^{(num)}(t, z)|$  and  $|\psi_{sq,n}^{(num)}(t, z)|$  on the time domain before and after shifting the frequency by the decomposition method. As can be seen, we have very good agreements between the numerical measurements and the theory predictions in Figs. 3[(a)-(c)], as well as between the pulse patterns before and after employing the frequency shifting in Fig. 3(d). We note that the theoretical predictions  $|\hat{\psi}_{sq}^{(th)}(\omega, z)|$  are measured from Eq. (2.10) with the values of  $\eta(z)$ ,  $\beta(z)$ ,  $y(z)$ , and  $\theta(z)$  are determined from the simulation.

*Discussion on the robustness of the procedure III.* It is worthy to emphasize that the decomposition method is very robust and simple to implement. Indeed, we can perfectly shift the frequency a value of  $\Delta\beta_1$  by the “naive” method without adjusting or approximating the value of  $\Delta\beta_1$  to fit with the grid size in the frequency domain. That is,  $\Delta\beta_1^{(num)} = \Delta\beta_1$  in simulations. In fact, we recall the following relation between the wavenumber separation in the frequency domain and the length of the time domain  $\Delta\omega = 2\pi/L_t$ , where  $L_t$  is the length of the computational time domain [32, 33]. Thus,



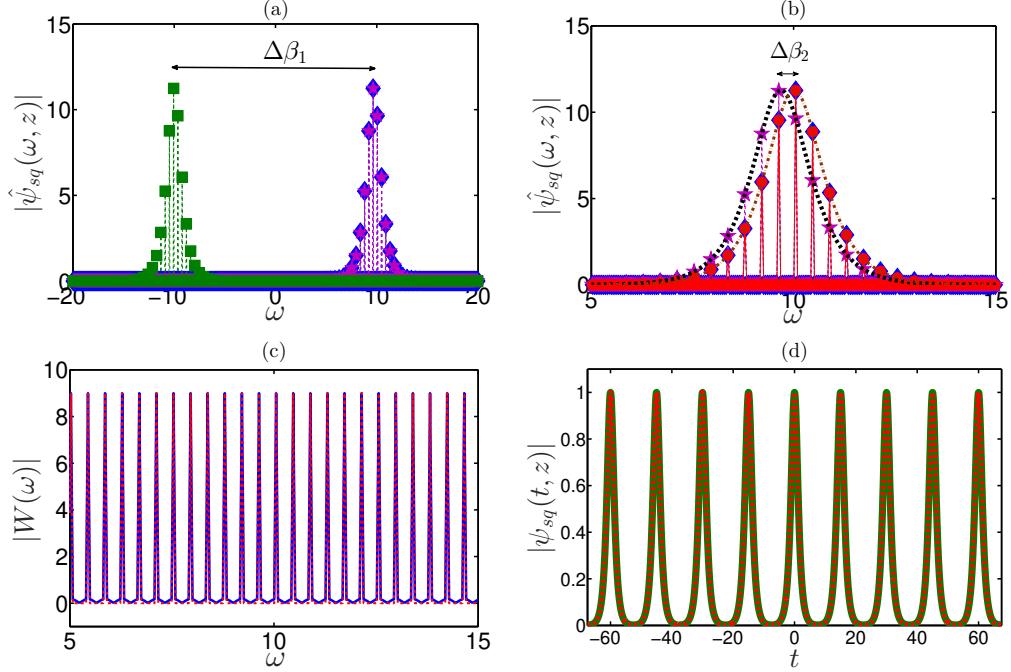


FIGURE 3. (Color online) The frequency shifting procedure using the decomposition method with  $\Delta\beta = 20$  at the propagation distance  $z = 5$ . (a) The pulse patterns in the frequency domain before and after employing the frequency shifting with  $\Delta\beta_1$ . The green squares represent  $|\hat{\psi}_{sq}^{(num)}(\omega, z)|$  before employing the frequency shifting. The purple stars and the blue diamonds correspond to  $|\hat{\psi}_{sq,n1}^{(num)}(\omega, z)|$  as obtained by Eq. (2.75) and its theoretical prediction  $|\hat{\psi}_{sq,n1}^{(th)}(\omega, z)|$ , respectively. (b) The purple stars are the same as in (a). The red circles and the blue diamonds represent  $|\hat{\psi}_{sq,n}^{(num)}(\omega, z)|$  as measured by Eq. (2.76) and its theoretical prediction  $|\hat{\psi}_{sq,n}^{(th)}(\omega, z)|$ , respectively. The black dashed and brown dashed-dotted curves represent  $\tilde{V}^{(num)}(\omega, z)$  and  $\tilde{V}_n^{(num)}(\omega, z)$  before and after shifting the frequency with  $\Delta\beta_2$  measured by Eq. (2.70), respectively. (c) The form of fast oscillation function  $|W(\omega)|$ . The red dashed and blue solid curves represent  $|W^{(num)}(\omega)|$  measured by Eq. (2.72) and its theoretical prediction  $|W^{(th)}(\omega)|$ , respectively. (d) The final soliton patterns in the time domain before and after employing the frequency shifting. The green solid and red dashed curves correspond to  $|\psi_{sq}^{(num)}(t, z)|$ , measured by the numerical simulation with Eq. (2.1), and  $|\psi_{sq,n}^{(num)}(t, z)|$  measured from the decomposition method, respectively.

in a closed fiber loop setup, we have  $\Delta\omega = 2\pi/[(2J+1)T]$ . As a result, the value of  $\Delta\beta_1$ , which is in form of  $2m\pi/T$ , is exactly a multiple of the wavenumber separation  $\Delta\omega$  in the frequency domain. That is, there exists a positive integer  $n = (2J+1)m$  such that  $\Delta\beta_1 = n\Delta\omega$ . Therefore, we can perfectly shift  $\Delta\beta_1$  by Eq. (2.75) without finding the nearest integer  $n$  such that  $\Delta\beta_1^{(num)} = n\Delta\omega$ .

### 3. APPLICATIONS OF FREQUENCY SHIFTING PROCEDURES

**3.1. Stabilization the propagation in waveguides with frequency dependent linear gain-loss.** We consider propagation of solitons in the presence of frequency dependent linear gain-loss

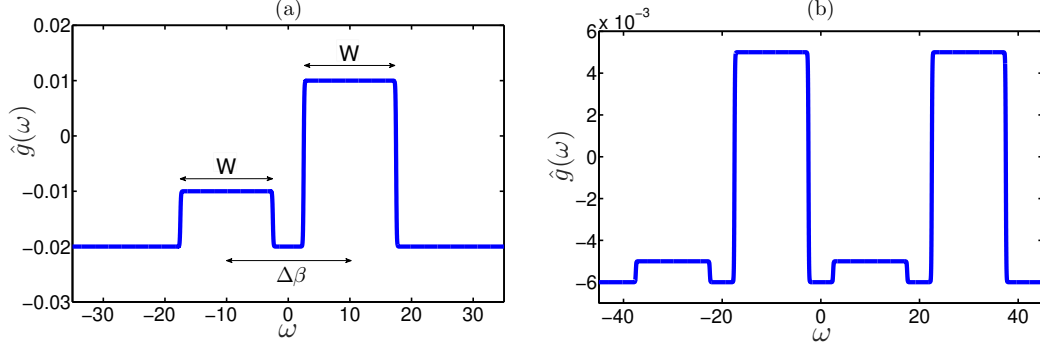


FIGURE 4. (Color online) The frequency shifting in the presence of frequency dependent linear gain-loss with  $\kappa = 1$  (a) and  $\kappa = 2$  (b). (a)  $\hat{g}(\omega)$  vs  $\omega$  in Eq. (3.32) with parameters used in setup 3 and used for Fig. 7. (b)  $\hat{g}(\omega)$  vs  $\omega$  in Eq. (3.24) with parameters used in setup 4a and used for Fig. 8.

[21, 22, 23]:

$$i\partial_z\psi + \partial_t^2\psi + 2|\psi|^2\psi = i\mathcal{F}^{-1} \left[ \hat{g}(\omega)\hat{\psi} \right] / 2, \quad (3.23)$$

where  $\hat{g}(\omega)$  is the linear gain-loss,  $\hat{\psi}$  is the FT of  $\psi$  with respect to time,  $\mathcal{F}^{-1}$  is the inverse FT [29]. We emphasize that similar forms of  $\hat{g}(\omega)$ , which are step-size functions, have been studied in Refs. [21, 22, 23]. In these papers, it has been shown that the use of frequency dependent linear gain-loss can suppress the radiative effects and stabilize soliton transmission to long distances instead of using constant gain-loss coefficients. In Eq. (3.23), the form of  $\hat{g}(\omega)$  is defined such that radiation emission effects are mitigated by the use of negative loss  $g_L$  in the frequency nearby the central frequency  $\beta(z)$ . In particular, we use the following continuous form with experiencing loss-gain  $\kappa$  times for  $\hat{g}(\omega)$ :

$$\hat{g}(\omega) = -g_L + 0.5 \sum_{j=0}^{2\kappa-1} \left\{ [(-1)^j g_0 + g_L] \sum_{k=0}^1 (-1)^k g_{j,k}(\omega) \right\}, \quad (3.24)$$

where  $g_{j,k}(\omega) = \tanh[\rho(\omega + (2j - 2\kappa + 1)\Delta\beta/2 + (-1)^k W/2)]$ ,  $0 < g_0 \ll 1$ ,  $g_L \geq 0$ ,  $\rho \gg 1$ , and the spectral width  $W$  satisfies  $1 \ll W \leq \Delta\beta$ . Physically,  $g_L$  is the loss required for suppressing radiation emission, while  $g_0$  is the gain required for maintaining stable propagation against decaying soliton amplitudes experiencing by the linear loss  $-g_0$ . We perform the multiple frequency shifting such that the solitons experience the linear gain or loss in the new shifted frequency and then continue propagating along the waveguide. By simulations, we shall show that the propagation of solitons is stable under the frequency shifting and the use of  $\hat{g}(\omega)$ .

As an example, Fig. 4 depicts a graph for  $\hat{g}(\omega)$  with  $\kappa = 1$  in Fig. 4(a) and  $\kappa = 2$  in Fig. 4(b), respectively. Let us describe the frequency shifting procedure for the use of  $\hat{g}(\omega)$  as in Fig. 4(a). Assume a sequence of solitons is propagating at the central frequency  $\beta = -10$  in the presence of the gain-loss function  $\hat{g}(\omega)$  as in Fig. 4(a). Thus, solitons experience the linear loss at the central frequency  $\beta = -10$  and the amplitude will be decreasing due to the linear loss. We perform the shifting the current frequency  $\beta = -10$  by  $\Delta\beta = 20$ , then the solitons will turn to experience the linear gain at the new central frequency of  $\beta_n = 10$ . We shall demonstrate that the propagation of a sequence of solitons described by Eq. (3.23) is stable under performing the frequency shifting, even with periodic shifting frequency multiple times as the use of  $\hat{g}(\omega)$  in Fig. 4(b). The setups will be studied in detail in section 4.

In rest of the current section, we theoretically derive the ODE describing the amplitude dynamics of a single soliton and a sequence of solitons in the presence of frequency dependent linear gain-loss in Eq. (3.23). This ODE can be used to verify the soliton dynamics in section 4.

First, we derive the equation for the amplitude dynamics of a single soliton described by Eq. (3.23). We consider the initial condition as in Eq. (2.3). We denote by  $z^*$  the complex conjugate of a complex number  $z$ . From Eq. (3.23), by deriving the energy balance, one can obtain

$$\partial_z \left[ \int_{-\infty}^{\infty} |\psi(t, z)|^2 dt \right] = I_1 + I_2, \quad (3.25)$$

where

$$I_1 = \frac{1}{2} \int_{-\infty}^{\infty} \psi^*(t, z) \mathcal{F}^{-1} \left[ \hat{g}(\omega) \hat{\psi}(\omega, z) \right] dt, \quad (3.26)$$

and

$$I_2 = \frac{1}{2} \int_{-\infty}^{\infty} \psi(t, z) \mathcal{F}^{-1} \left[ \hat{g}^*(\omega) \hat{\psi}^*(\omega, z) \right] dt. \quad (3.27)$$

In order to solve Eq. (3.25), we employ the adiabatic perturbation method, which was developed by Kaup [34, 35], and has been extensively used to study soliton dynamics, see, for example, Refs. [19, 25, 28, 31]. In this method, one can determine the effects of small dissipations on the evolution of parameters by the exactly solvable NLS, that is, by using Eq. (2.4) for the soliton part. This calculation yields

$$2 \frac{d\eta}{dz} = I_1 + I_2, \quad (3.28)$$

where  $I_1$  and  $I_2$ , by the convolution theorem for the inverse FT, are simplified by

$$I_1 = \frac{\eta^2}{2(2\pi)^{1/2}} \int_{-\infty}^{\infty} \frac{dt}{\cosh[\eta(t - y(z))]} \int_{-\infty}^{\infty} \frac{g(s) e^{-i\beta s} ds}{\cosh[\eta(t - s - y(z))]}, \quad (3.29)$$

and

$$I_2 = \frac{\eta^2}{2(2\pi)^{1/2}} \int_{-\infty}^{\infty} \frac{dt}{\cosh[\eta(t - y(z))]} \int_{-\infty}^{\infty} \frac{g^*(s) e^{i\beta s} ds}{\cosh[\eta(t - s - y(z))]}. \quad (3.30)$$

From Eqs. (3.28)-(3.30), we obtain

$$\frac{d\eta}{dz} = \frac{\eta}{4(2\pi)^{1/2}} \int_{-\infty}^{\infty} \frac{dv}{\cosh(v)} \int_{-\infty}^{\infty} \frac{g(s) e^{-i\beta s} + g^*(s) e^{i\beta s}}{\cosh(v - \eta s)} ds, \quad (3.31)$$

where  $v = \eta(t - y(z))$ . Equation (3.31) described the amplitude dynamics of a soliton of Eq. (3.23).

Second, we simplify Eq. (3.31) for a specific form of  $\hat{g}(\omega)$ . For simple, we consider  $\kappa = 1$  and  $\beta(0) = -\Delta\beta/2$ . Then  $\hat{g}(\omega)$  has the form

$$\begin{aligned} \hat{g}(\omega) = & -g_L + 0.5(-g_0 + g_L) \{ \tanh[\rho(\omega + b)] - \tanh[\rho(\omega + a)] \} \\ & + 0.5(g_0 + g_L) \{ \tanh[\rho(\omega - a)] - \tanh[\rho(\omega - b)] \}, \end{aligned} \quad (3.32)$$

where  $a = (\Delta\beta - W)/2$  and  $b = (\Delta\beta + W)/2$  (see, for example, Fig. 4 (a)). We note that in the limit as  $\rho \gg 1$ ,  $\hat{g}(\omega)$  can be approximated by the following function:

$$\hat{g}(\omega) = \begin{cases} -g_0, & \text{if } -\Delta\beta/2 - W/2 < \omega < -\Delta\beta/2 + W/2, \\ g_0, & \text{if } \Delta\beta/2 - W/2 < \omega < \Delta\beta/2 + W/2, \\ -g_L, & \text{elsewhere.} \end{cases} \quad (3.33)$$

Without loss of generality, we assume that the current frequency of the soliton is  $\beta \simeq \beta(0) = -\Delta\beta/2$ . That is, the soliton is currently experienced the linear loss before shifting the frequency, and thus

the frequency after shifting the frequency is  $\beta + \Delta\beta = \Delta\beta/2$ . From Eq. (3.33), by calculating  $\mathcal{F}^{-1}(\hat{g}(\omega))$ , it yields

$$g(t) = -(2\pi)^{1/2} g_L \delta(t) + (2/\pi)^{1/2} (g_L - g_0) e^{-i\Delta\beta t/2} \sin(Wt/2)/t \\ + (2/\pi)^{1/2} (g_L + g_0) e^{i\Delta\beta t/2} \sin(Wt/2)/t, \quad (3.34)$$

where  $\delta(t)$  is the Dirac delta function. Substitute Eq. (3.34) into Eq. (3.31) and simplify, we get the ODE for the amplitude dynamics:

$$\frac{d\eta}{dz} = -\frac{g_L \eta}{2} J_1 + \frac{(g_L - g_0) \eta}{2\pi} J_2 + \frac{(g_L + g_0) \eta}{2\pi} J_3, \quad (3.35)$$

where

$$J_1 = \int_{-\infty}^{\infty} \frac{dv}{\cosh(v)} \int_{-\infty}^{\infty} \frac{\delta(s) \cos(\beta s)}{\cosh(v - \eta s)} ds = \int_{-\infty}^{\infty} \frac{dv}{\cosh^2(v)} = 2, \quad (3.36)$$

$$J_2 = \int_{-\infty}^{\infty} \frac{dv}{\cosh(v)} \int_{-\infty}^{\infty} \frac{\sin(Ws/2)}{\cosh(v - \eta s) s} ds, \quad (3.37)$$

and

$$J_3 = \int_{-\infty}^{\infty} \frac{dv}{\cosh(v)} \int_{-\infty}^{\infty} \frac{\cos(\Delta\beta s) \sin(Ws/2)}{\cosh(v - \eta s) s} ds. \quad (3.38)$$

We now calculate  $J_2$  and  $J_3$ . We note that

$$J_2 = \int_{-\infty}^{\infty} \frac{\sin(Ws/2) ds}{s} \int_{-\infty}^{\infty} \frac{dv}{\cosh(v) \cosh(v - \eta s)}. \quad (3.39)$$

By using identity 2.444(1) and 3.981(1) in [36], we arrive

$$J_2 = 2\eta \int_{-\infty}^{\infty} \frac{\sin(Ws/2)}{\sinh(\eta s)} ds = 2\pi \tanh\left(\frac{\pi W}{4\eta}\right). \quad (3.40)$$

On the other hand, by using identity 2.444(1) in [36], we also have

$$J_3 = 2\eta \int_{-\infty}^{\infty} \frac{\cos(\Delta\beta s) \sin(Ws/2)}{\sinh(\eta s)} ds. \quad (3.41)$$

It implies

$$J_3 = 2\eta \int_0^{\infty} \frac{\sin[(\Delta\beta + W/2)s]}{\sinh(\eta s)} ds - 2\eta \int_0^{\infty} \frac{\sin[(\Delta\beta - W/2)s]}{\sinh(\eta s)} ds. \quad (3.42)$$

By using identity 3.981(1) in [36], we have

$$J_3 = \pi \left[ \tanh\left(\frac{\pi(2\Delta\beta + W)}{4\eta}\right) - \tanh\left(\frac{\pi(2\Delta\beta - W)}{4\eta}\right) \right]. \quad (3.43)$$

Substituting  $J_1$ ,  $J_2$ , and  $J_3$  into Eq. (3.35), one can obtain the ODE for the amplitude dynamics:

$$\frac{d\eta}{dz} = -g_L \eta + (-g_0 + g_L) \eta \tanh\left(\frac{\pi W}{4\eta}\right) \\ + \frac{\eta}{2} (g_0 + g_L) \left[ \tanh\left(\frac{\pi(2\Delta\beta + W)}{4\eta}\right) - \tanh\left(\frac{\pi(2\Delta\beta - W)}{4\eta}\right) \right]. \quad (3.44)$$

This approximate ODE describes the amplitude dynamics of a soliton experienced the linear loss before shifting the frequency. If  $2\Delta\beta + W \gg 1$  and  $2\Delta\beta - W \gg 1$ , then one can neglect the 3rd and 4th terms of the RHS of Eq. (3.44). Therefore,

$$\frac{d\eta}{dz} = -g_L \eta + (-g_0 + g_L) \eta \tanh\left(\frac{\pi W}{4\eta}\right). \quad (3.45)$$

Similarly, an approximated ODE for the amplitude dynamics of a soliton experienced the linear gain after each frequency shifting is

$$\frac{d\eta}{dz} = -g_L\eta + (g_0 + g_L)\eta \tanh\left(\frac{\pi W}{4\eta}\right). \quad (3.46)$$

Next, we derive the equation for the amplitude dynamics of a *sequence* of solitons propagating in the presence of frequency dependent linear gain-loss in Eq. (3.23). We consider the initial condition as in Eq. (2.8). By the adiabatic perturbation method, we turn to consider the soliton sequence solution of Eq. (3.23) in form of Eq. (2.9). The  $k^{\text{th}}$  soliton of this sequence of solitons is

$$\psi_{sq}^{(k)}(t, z) = \eta(z)e^{i\theta(z)} \frac{\exp\{i\beta(z)[t - y(z) - kT]\}}{\cosh\{\eta(z)[t - y(z) - kT]\}}. \quad (3.47)$$

Similarly to the derivation of the amplitude dynamics for a single soliton, we obtain an approximated ODE for the amplitude dynamics of the  $k^{\text{th}}$  soliton experienced the linear loss before each frequency shifting as in Eq. (3.45) and linear gain after each frequency shifting as in Eq. (3.46). Therefore, an approximated ODE for the amplitude dynamics of a sequence of solitons experienced the linear loss before each frequency shifting and the linear gain after each frequency shifting is as in Eq. (3.45) and Eq. (3.46), respectively. The ODE for amplitude dynamics can be used to verify the robust propagation of a sequence of solitons in section 4.

**3.2. Repeated soliton collisions in waveguides with cubic loss.** In this section, we demonstrate the use of the frequency shift to enable repeated two-soliton collisions in the presence of weak cubic loss and measure the theoretical prediction for the accumulative amplitude shift. The propagation equation in terms of coupled NLS equation is [22]

$$i\partial_z\psi_j + \partial_t^2\psi_j + 2|\psi_j|^2\psi_j + 4|\psi_k|^2\psi_j = -i\epsilon_3|\psi_j|^2\psi_j - 2i\epsilon_3|\psi_k|^2\psi_j, \quad (3.48)$$

where  $\epsilon_3$  is the weak cubic loss coefficient ( $0 < \epsilon_3 \ll 1$ ),  $\psi_j$  is the electric field's envelope for the  $j^{\text{th}}$  soliton,  $j = 1, 2$ . The third and the fourth terms on the left hand side of Eq. (3.48) describe the effects of intrasequence and intersequence interaction due to Kerr nonlinearity, respectively. The first and the second terms on the right hand side of Eq. (3.48) describe intrasequence and intersequence interaction due to cubic loss, respectively.

The initial conditions are

$$\psi_1(t, 0) = \frac{\eta_1(0)}{\cosh[\eta_1(0)t]}, \quad \psi_2(t, 0) = \frac{\eta_2(0) \exp[i\beta(0)t]}{\cosh[\eta_2(0)(t - y_2(0))]}, \quad (3.49)$$

where  $\beta(0) > 0$  and  $y_2(0) < 0$  such that two solitons are initially well separated, for example,  $y_2(0) = -20$ . That is, soliton 1 is a standing wave and soliton 2 is located at  $y_2(0) < 0$  on the left with the group velocity of  $v_g = 2\beta(0) > 0$ . Therefore, there will be a two-soliton collision at the propagation distance  $z_{c1} = -y_2(0)/[2\beta(0)]$ .

The idea of using the frequency shift for repeating soliton collisions is to change their group velocity. First, we employ the frequency shift procedure for solitons as follows. Two solitons are well separated at the propagation distance  $z_{s1} = 2z_{c1}$ . We now abruptly change their group velocity by employing the 1<sup>st</sup> frequency shifting of the value  $\Delta\beta = \beta(0)$  at the propagation distance  $z_{s1}$  such that

$$\hat{\psi}_1(\omega, z_{s1}) \rightarrow \hat{\psi}_{n1}(\omega - \beta(0), z_{s1}), \quad (3.50)$$

and

$$\hat{\psi}_2(\omega, z_{s1}) \rightarrow \hat{\psi}_{n2}(\omega + \beta(0), z_{s1}). \quad (3.51)$$

Therefore, after the 1<sup>st</sup> frequency shifting, soliton 1 is going to the right and going to collide with soliton 2, which currently becomes a standing wave. Let  $z_{c_j}$  be the propagation distance of the  $j^{\text{th}}$  collision. The propagation distance of the 2<sup>nd</sup> collision thus is

$$z_{c_2} = -3y_2(0)/[2\beta(0)]. \quad (3.52)$$

Similarly, we continue employing the frequency shifting of size  $\beta(0)$  at  $z_{s_2} = 2z_{s_1}$  such that

$$\hat{\psi}_1(\omega, z_{s_2}) \rightarrow \hat{\psi}_{n1}(\omega + \beta(0), z_{s_2}), \quad (3.53)$$

and

$$\hat{\psi}_2(\omega, z_{s_2}) \rightarrow \hat{\psi}_{n2}(\omega - \beta(0), z_{s_2}). \quad (3.54)$$

We repeat this process  $n$  times. We obtain that the  $n^{\text{th}}$  collision distance is thus located at

$$z_{c_n} = -(2n - 1)y_2(0)/[2\beta(0)], \quad (3.55)$$

and the  $n^{\text{th}}$  frequency shifting distance is

$$z_{s_n} = nz_{s_1} = -ny_2(0)/\beta(0). \quad (3.56)$$

In Fig. 10, we illustrate an example for repeating soliton collision by employing the frequency shift.

Second, we calculate the theoretical collision-induced amplitude shift. If we neglect the frequency shift due to weak perturbations, then we can suppose that  $\beta(z) = \beta \simeq \beta(0)$ . We recall that the dynamics of solitons in the presence of weak cubic loss is given by [25]

$$\eta_j(z) = \eta_j(z_0) [1 + 8\epsilon_3\eta_j^2(z_0)(z - z_0)/3]^{-1/2}, \quad (3.57)$$

for  $z > z_0$ , and the collision-induced amplitude shift on the  $j^{\text{th}}$  soliton at the propagation distance  $z_c$  is [25]

$$\Delta\eta_j^{(c)} = -4\epsilon_3\eta_j(z_c)\eta_k(z_c)/|\beta|. \quad (3.58)$$

The total of collision-induced amplitude shift can be theoretically measured by the following procedure. The amplitude shift induced by the first collision is

$$\Delta\eta_j^{(c_1)} = -4\epsilon_3\eta_1(z_{c_1}^-)\eta_2(z_{c_1}^-)/|\beta|, \quad (3.59)$$

where the soliton amplitude before the 1<sup>st</sup> collision  $\eta_j(z_{c_1}^-)$  is calculated from  $\eta_j(0)$  by Eq. (3.57). For  $k \geq 2$ ,  $\eta_j(z_{c_k}^-)$  is also calculated by

$$\eta_j(z_{c_k}^-) = \eta_j(z_{c_{k-1}}^+) [1 + 8\epsilon_3\eta_j^2(z_{c_{k-1}}^+)(z_{c_k} - z_{c_{k-1}})/3]^{-1/2}, \quad (3.60)$$

where  $\eta_j(z_{c_{k-1}}^+) = \eta_j(z_{c_{k-1}}^-) - \Delta\eta_j^{(c_{k-1})}$  is the soliton amplitude after the  $(k-1)^{\text{th}}$  collision. Therefore, the  $k^{\text{th}}$  collision-induced amplitude shift is calculated by

$$\Delta\eta_j^{(c_k)} = -4\epsilon_3\eta_1(z_{c_k}^-)\eta_2(z_{c_k}^-)/|\beta|, \quad (3.61)$$

where  $\eta_j(z_{c_k}^-)$  is defined by Eq. (3.60). Therefore, one can obtain the total of collision-induced amplitude shift after  $n$  collisions  $\Delta\eta_j^{(c)}$  as follows:

$$\Delta\eta_j^{(c)} = \sum_{k=1}^n \Delta\eta_j^{(c_k)}, \quad (3.62)$$

where  $\Delta\eta_j^{(c_k)}$  is defined by Eq. (3.61),  $j = 1, 2$ .



Third, we describe the numerical implementation for measuring the value of the accumulative collision-induced amplitude shift in simulations. We note that the  $z$  dependence of the soliton amplitude on  $[z_{c_k}^+, z_{c_{k+1}}^-]$  is

$$\eta_j(z) = \eta_j(z_{c_k}^+) [1 + 8\epsilon_3 \eta_j^2(z_{c_k}^+)(z - z_{c_k}^+)/3]^{-1/2}, \quad (3.63)$$

where  $k \geq 1$ . The  $k^{\text{th}}$  collision-induced amplitude shift can be numerically calculated by

$$\Delta\eta_j^{(c_k)(num)} = \eta_j(z_{c_k}^+) - \eta_j(z_{c_k}^-), \quad (3.64)$$

where  $\eta_j(z_{c_k}^-)$  and  $\eta_j(z_{c_k}^+)$  are measured by

$$\eta_j(z_{c_k}^-) = \eta_j(z_{s_{k-1}}) [1 + 8\epsilon_3 \eta_j^2(z_{s_{k-1}})(z_{c_k} - z_{s_{k-1}})/3]^{-1/2}, \quad (3.65)$$

and

$$\eta_j(z_{c_k}^+) = \eta_j(z_{s_k}) [1 - 8\epsilon_3 \eta_j^2(z_{s_k})(z_{s_k} - z_{c_k})/3]^{-1/2}, \quad (3.66)$$

where  $\eta_j(z_{s_k})$  is measured from the numerical simulation of Eq. (3.48). The numerical value of the accumulative collision-induced amplitude shift after  $n$  collisions  $\Delta\eta_j^{(c)(num)}$  is calculated as follows:

$$\Delta\eta_j^{(c)(num)} = \sum_{k=1}^n \Delta\eta_j^{(c_k)(num)}, \quad (3.67)$$

where  $j = 1, 2$ .

#### 4. NUMERICAL SIMULATIONS

In this section, we present the simulation results for frequency shifting procedures of a single soliton and of a sequence of solitons, and their applications. The cubic NLS equation Eq. (2.1), Eq. (3.23), and Eq. (3.48) are numerically solved by using the split-step Fourier method (see Appendix C).

**4.1. Numerical simulations for frequency shifting procedures.** We first present the numerical simulation with Eq. (2.1) for the frequency shifting procedure of a single soliton in a large time-domain and then compare the numerical results with the theoretical predictions. To illustrate the frequency shift for a single soliton, we consider the numerical **setup 1** with following parameters:  $\Delta\beta = 20$ ,  $\beta(0) = -160$ ,  $y(0) = 360$ ,  $\eta(0) = 1$ ,  $\alpha(0) = 0$ ,  $\Delta z = 0.0001$ ,  $\Delta t = 0.018$ ,  $t_{\max} = 380$ ,  $t_{\min} = -t_{\max}$ , and  $z_s = 0.5$  [29]. We have the numerical measurements:  $\Delta\omega = 0.00826735$ ,  $\Delta\beta^{(num)} = 19.9987$ , and  $n_{shift} = 2419$ . The  $k^{\text{th}}$  frequency shift is implemented at the propagation distances  $z_{s_k} = kz_s = 0.5k$  with  $k$  is a positive integer. Figures 5(a) and 5(b) represent the pulse patterns in the time domain and in the frequency domain, respectively, after the 16<sup>th</sup> frequency shifting ( $k = 16$ ). As can be seen, the pulse shapes measured from the simulation with Eq. (2.1) and Eq. (1.68) are in very good agreement with their theoretical predictions with  $\beta^{(num)}(z = 8) = 159.979$ .

Second, we present the numerical simulation with Eq. (2.1) for the frequency shifting procedure of a sequence of solitons with the decomposition method and then compare the numerical results with the theoretical predictions. Here we choose to illustrate the frequency shifting procedure for a waveguide loop setup. The NLS equation (2.1) is numerically solved by using the split-step Fourier method with periodic boundary conditions [6]. The use of periodic boundary conditions means that the numerical simulations describe soliton dynamics in a closed waveguide loop. The initial condition is in the form of a periodic sequence of  $2J + 1$  solitons with initial amplitudes  $\eta(0)$  and initial frequencies  $\beta(0)$  as described in Eq. (2.9). We consider **setup 2** with parameters as follows:  $\Delta\beta = 20$ ,  $L = 15$ ,  $\eta(0) = 1$ ,  $\beta(0) = -160$ ,  $y(0) = -5$ ,  $\alpha(0) = 0$ ,  $T = 15$ ,  $J = 4$ ,

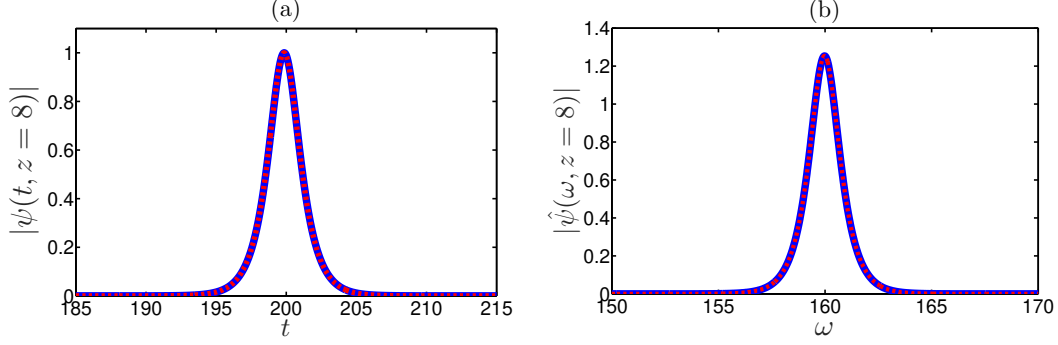


FIGURE 5. (Color online) Multiple frequency shifting for a single soliton in a large time domain. The pulse patterns are in the time domain (a) and in the frequency domain (b) at the distance  $z = 8$  after performing 16 shifts of the frequency with parameters in setup 1. The red dashed curve corresponds to  $|\psi(t, z)|$  obtained by the numerical simulation with Eq. (2.1) and the frequency shifting procedure for a single soliton (a), or its FT  $|\hat{\psi}(\omega, z)|$  (b). The blue solid curve represents the theoretical prediction for  $|\psi(t, z)|$  (a), or its FT  $|\hat{\psi}(\omega, z)|$  (b) obtained from Eq. (1.69).

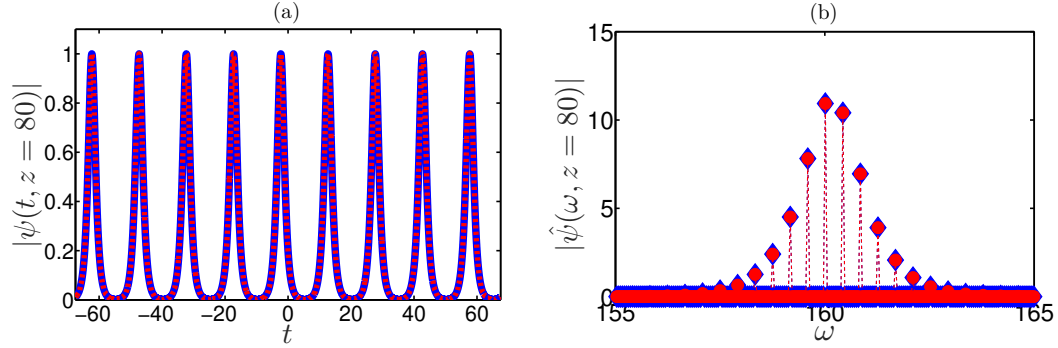


FIGURE 6. (Color online) Multiple frequency shifting for a sequence of solitons by the decomposition method. The soliton patterns are in the time domain (a) and in the frequency domain (b) at the distance  $z = 80$  after performing 16 shifts of the frequency with parameters in setup 2. (a) The red dashed and blue solid curves correspond to  $|\psi(t, z)|$  obtained by numerical simulation with Eq. (2.1) and its theoretical prediction. (b) The red circles and blue diamonds represent  $|\hat{\psi}(\omega, z)|$  and its theoretical prediction.

$\Delta z = 0.0001$ ,  $\Delta t = 0.018$ ,  $t_{\max} = 67.5$ ,  $t_{\min} = -t_{\max}$ , and  $z_s = 5$  [29]. We then have  $\Delta\omega = 0.0465$  and  $\Delta\beta^{(num)} = 20.0131$  ( $n_{shift} = 430$ ) that consists  $\Delta\beta_1 = 94\pi/T = 19.6873$  ( $n_{shift} = 423$ ) and  $\Delta\beta_2 = 0.3258$  ( $n_{shift} = 7$ ). The  $k^{\text{th}}$  frequency shifting is implemented at the propagation distances  $z_{s_k} = kz_s = 5k$  with  $k \in \mathbb{Z}^+$ . Figures 6(a) and 6(b) represent the soliton patterns in the time domain and in the frequency domain, respectively, after the 16<sup>th</sup> shifting of frequency. It is seen that the pulse patterns are still in excellent shapes. The numerical measurement for the frequency after the 16<sup>th</sup> frequency shifting is  $\beta^{(num)}(z = 80) = 160.172$ . The very good agreement between the results of the numerical simulations and the theoretical predictions confirms the robustness of the frequency shifting procedure for a sequence of solitons.

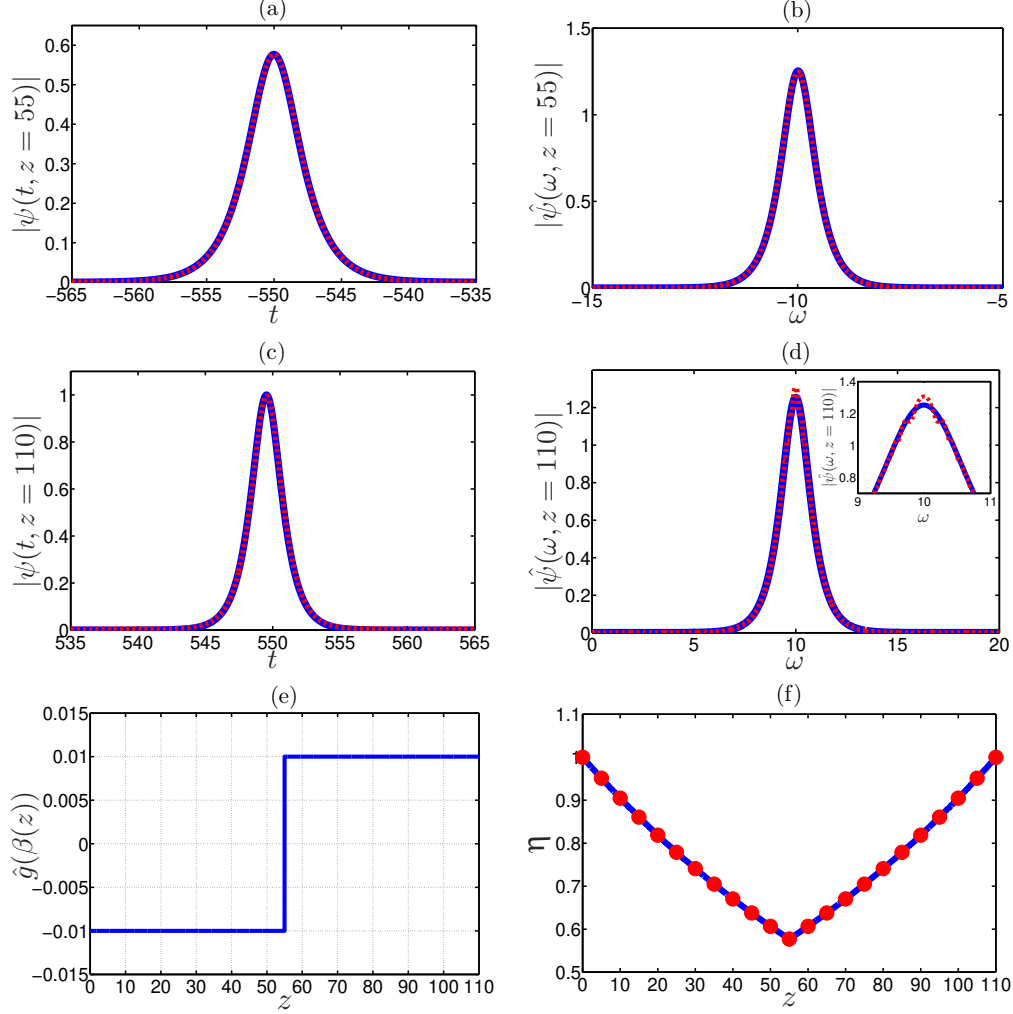


FIGURE 7. (Color online) Single frequency shifting in the presence of frequency dependent linear gain-loss for a single soliton ( $\kappa = 1$ ). The soliton patterns are in the time domain and in the frequency domain at the end of loss period  $z = 55$  [(a)-(b)] and at the end of gain period  $z = 110$  [(c)-(d)] with parameters in setup 3. The red dashed curve represents  $|\psi(t, z)|$  obtained by numerical simulation with Eq. (3.23) and Eq. (3.32) or its FT  $|\hat{\psi}(\omega, z)|$  at  $z = 55$  [(a)-(b)] and at the distance  $z = 110$  [(c)-(d)], respectively. The blue solid curve corresponds to the theoretical prediction for  $|\psi(t, z)|$  or  $|\hat{\psi}(\omega, z)|$  at the distance  $z = 55$  [(a) - (b)] and the distance  $z = 110$  [(c) - (d)], respectively. The inset at the upper right of (d) is a magnified version of the pulse pattern on the top. (e) The  $z$  dependence of  $\hat{g}(\beta(z))$  in Eq. (3.32). (f) The  $z$  dependence of the soliton amplitude. The red circles and blue solid curve represent the amplitude  $\eta(z)$  obtained by Eq. (3.23) and Eq. (3.32) and its theoretical prediction obtained by Eq. (3.45) and Eq. (3.46).

**4.2. Numerical simulations for soliton propagations with frequency dependent linear gain-loss.** First, we present the single frequency shifting ( $\kappa = 1$ ) in the presence of frequency dependent linear gain-loss for a single soliton. That is, we implement the frequency shift such that the soliton will experience gain at the new frequency. The numerical simulation is implemented with

Eq. (3.23) and  $\hat{g}(\omega)$  as in Eq. (3.32). The parameters for  $\hat{g}(\omega)$  in **setup 3** are  $g_0 = 0.01$ ,  $g_L = 0.02$ ,  $\Delta\beta = 20$ ,  $W = 15$ , and  $\rho = 10$ . This function  $\hat{g}(\omega)$  is presented in Fig. 4(a). Other parameters are as follows:  $\beta(0) = -\Delta\beta/2 = -10$ ,  $y_0 = 550$ ,  $\eta_0 = 1$ ,  $\alpha(0) = 0$ ,  $\Delta z = 0.001$ ,  $\Delta t = 0.0588$ ,  $t_{\max} = 570$ ,  $t_{\min} = -t_{\max}$ , and  $z_s = 55$ . We implement the single frequency shifting by  $\Delta\beta$  at the distance  $z_s = 55$ . Therefore, the soliton is experienced the linear loss over the propagation distance  $[0, z_s] = [0, 55]$  and experienced the linear gain over the propagation distance  $[z_s, z_f]$ . The results are presented in Fig. 7. Figures 7(a) and 7(b) illustrate the soliton patterns at the distance  $z_s = 55$  (end of the loss period). Figures 7(c) and 7(d) show the soliton patterns at the final propagation distance  $z_f = 110$  (end of the gain period). The inset at the upper right corner of Fig. 7(d) shows a magnified version of the pulse pattern on the top. Figure 7(e) presents the profile of  $\hat{g}(\beta(z))$  vs.  $z$  to illustrate the propagation of solitons experienced different linear gain and loss at their central frequencies, as they propagate along the waveguide, while Fig. 7(f) presents the amplitude dynamics  $\eta(z)$ . It is seen that the agreement between the amplitude dynamics  $\eta(z)$  measured by the numerical simulation and the analytic prediction obtained from Eq. (3.45) and Eq. (3.46) is very good (Fig. 7(f)). We observe that there is a small instability of the pulse pattern in the frequency domain slightly arising at the final propagation distance  $z = z_f$  (see the inset at the upper right of Fig. 7(d)). Moreover, by extensively employing simulations for different values of  $g_0$ , we observe that the instability of the pulse pattern at the final propagation distance  $z = z_f$  depends on the magnitude of  $g_0$  and  $\eta(z_s)$ . More specifically, if  $g_0$  is very small,  $0.002 \leq g_0 \leq 0.05$ , and the amplitude at the end of loss period  $\eta(z_s)$  is pretty large,  $0.8 \leq \eta(z_s) \leq 1$ , then there are no instabilities at the distance  $z = z_f$ . If  $g_0$  is very small,  $0.002 \leq g_0 \leq 0.05$ , and  $\eta(z_s)$  is pretty small,  $0.4 \leq \eta(z_s) \leq 0.7$ , then instabilities are very weak and are gradually stabilized.

Second, we implement multiple periodic frequency shifting in the presence of frequency dependent linear gain-loss for a single soliton and for a sequence of solitons such that the solitons experience loss-gain  $\kappa$  times during a certain propagation distance. The numerical simulations are implemented with Eq. (3.23) and  $\hat{g}(\omega)$  as in Eq. (3.24) with  $\kappa = 2$ . We consider two setups: setup 4a for a single soliton and setup 4b for a sequence of solitons. The parameters of  $\hat{g}(\omega)$  for **Setup 4a** are:  $g_0 = 0.005$ ,  $g_L = 0.006$ ,  $\Delta\beta = 20$ ,  $W = 15$ ,  $\rho = 10$ , and  $\kappa = 2$ . This function  $\hat{g}(\omega)$  is presented in Fig. 4(b). Other parameters are:  $\beta(0) = -3\Delta\beta/2 = -30$ ,  $\eta_0 = 1$ ,  $y(0) = 2400$ ,  $\alpha(0) = 0$ ,  $\Delta z = 0.001$ ,  $\Delta t = 0.0588$ ,  $t_{\max} = 2415$ ,  $t_{\min} = -t_{\max}$ , and  $z_{s_k} = 60k$  with  $k = 1, 2, 3$ . That is, we implement the frequency shift at the distances  $z = 60, 120, 180$ . Solitons are experienced the processes of the linear loss-gain-loss-gain, respectively, over the propagation distance  $0 \leq z \leq z_f = 240$ . The numerical simulation results are presented in Fig. 8. Figures 8(a) and 8(b) show the soliton patterns at the final propagation distance  $z_f = 240$  in the time domain and the frequency domain, respectively. Figure 8(c) presents the frequency dependent gain-loss function  $\hat{g}(\beta(z))$  vs.  $z$  used along the fiber while Fig. 8(d) shows the amplitude dynamics  $\eta(z)$ . The parameters of  $\hat{g}(\omega)$  for **Setup 4b** are  $g_0 = 0.003$ ,  $g_L = 0.005$ ,  $\Delta\beta = 20$ ,  $W = 15$ ,  $\rho = 10$ , and  $\kappa = 2$ . Other parameters are:  $\beta(0) = -3\Delta\beta/2 = -30$ ,  $\eta(0) = 1$ ,  $y(0) = -5$ ,  $\alpha(0) = 0$ ,  $L = 15$ ,  $T = 15$ ,  $J = 4$ ,  $\Delta z = 0.001$ ,  $\Delta t = 0.0588$ ,  $t_{\max} = 67.5$ ,  $t_{\min} = -t_{\max}$ , and  $z_{s_k} = 250k$  with  $k = 1, 2, 3$ . That is, we implement the multiple frequency shifting by  $\Delta\beta$  at the distances  $z_{s_k} = 250, 500, 750$ . The numerical simulation results are shown in Fig. 9. The soliton patterns at the final propagation distance  $z_f = 1000$  are presented in the time domain in Fig. 9(a) and in the frequency domain in Fig. 9(b). Figure 9(c) presents  $\hat{g}(\beta(z))$  vs.  $z$  while Fig. 9(d) shows the amplitude dynamics  $\eta(z)$ . As can be seen, the pulse shapes obtained from numerical simulations and their theoretical predictions are in very good agreement, see Figs. 8(a)-(b) for a single soliton and Figs. 9(a)-(b) for a sequence of solitons. Additionally, the agreement between the amplitude dynamics  $\eta(z)$  measured by the numerical simulations and the analytic predictions is very good, see Fig. 8(d) for a single soliton and Fig. 9(d) for a sequence of solitons. Moreover, we observe that for a single soliton, instabilities eventually grow at the distance  $z = z_f/2$  by the linear gain and they are significantly

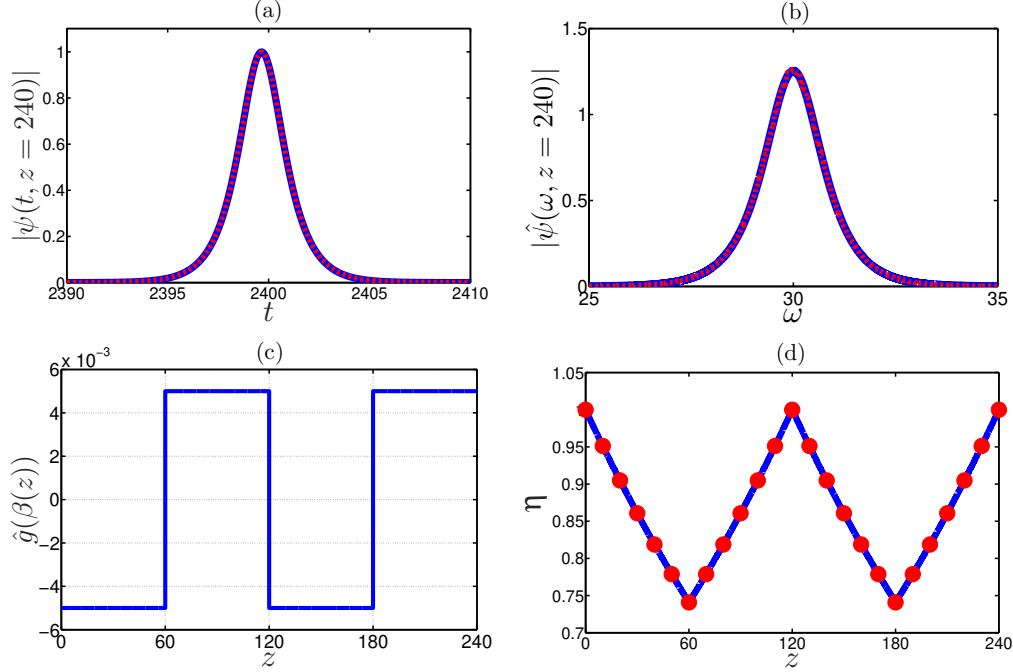


FIGURE 8. (Color online) Multiple frequency shifting periodically in the presence of frequency dependent linear gain-loss for a single soliton ( $\kappa = 2$ ) with parameters in setup 4a. (a)-(b) The soliton patterns in the time domain and the frequency domain at the final propagation distance  $z_f = 240$ , respectively. The red dashed and blue solid curves represent numerical results obtained from the numerical simulation with Eq. (3.23) and Eq. (3.24) and its theoretical prediction, respectively. (c) The  $z$  dependence of  $\hat{g}(\beta(z))$  in Eq (3.24). (d) The  $z$  dependence of the soliton amplitude. The red circles represent the numerical soliton amplitude  $\eta(z)$  measured by Eq. (3.23) and Eq. (3.24) while the blue solid curve corresponds to the theoretical prediction for  $\eta(z)$  measured by Eq. (3.45) and Eq. (3.46).

suppressed at  $z = 3z_f/4$  by the linear loss. The single soliton is in very good shape at the final propagation distance  $z_f = 240$ . For a sequence of solitons, we observe that the solitons are in very good shape at the very large propagation distance  $z_f = 1000$  as in Figs. 9(a)-(b). The instabilities are gradually suppressed during the long propagation distance.

In summary, we have the good shape of solitons and the very good agreement of amplitude dynamics between the simulation results and the theoretical predictions over a wide range of the amplitudes. These confirm that the propagation of solitons with implementing multiple frequency shifting in the presence of frequency dependent linear gain-loss is stable over intermediate to long distances. We emphasize that the soliton dynamics presented in Fig. 9(d) can be used for switching soliton dynamics or for transmission recovery. In these switching processes, one can turn off (or turn on) a sequence of solitons by guiding its amplitude below (or above) a threshold amplitude value  $\eta_{th}$  (see [22, 28] for another approach to study the switching dynamics by using hybrid waveguides and stability analysis of the equilibrium states of the ODEs describing amplitude dynamics). The amplitude threshold value in Fig. 9(d) can be, for example,  $\eta_{th} = 0.5$ .

**4.3. Numerical simulations for repeating soliton collisions with weak cubic loss.** In this section, we present simulations for the use of the frequency shifting to repeated two-soliton collisions. We then numerically measure the value of the accumulative collision-induced amplitude shift

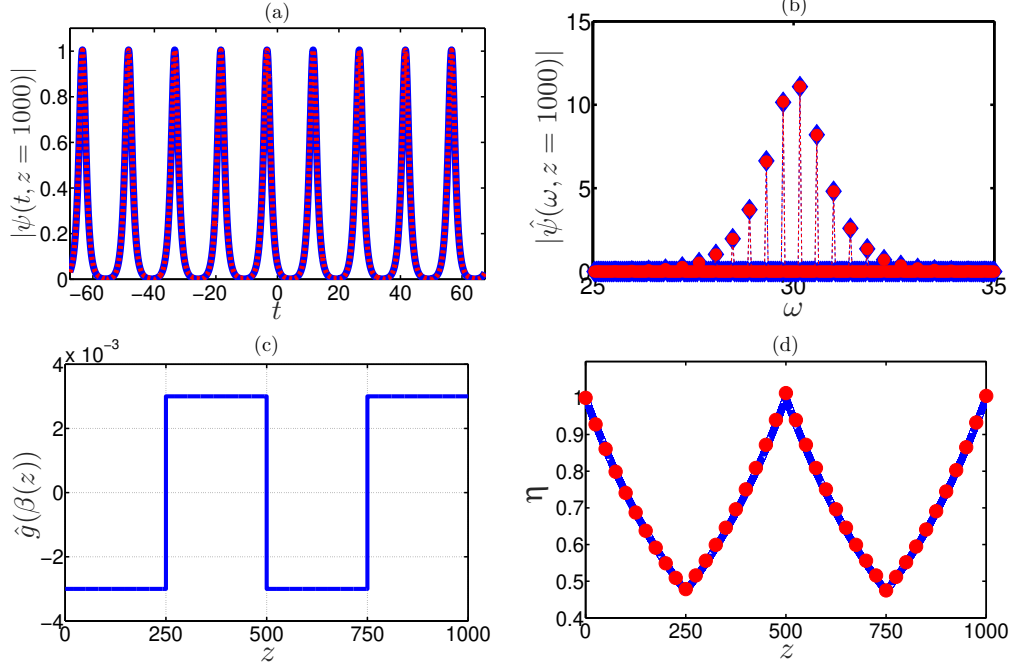


FIGURE 9. (Color online) Multiple frequency shifting periodically in the presence of frequency dependent linear gain-loss for a sequence of solitons ( $\kappa = 2$ ) with parameters in setup 4b. (a) The soliton patterns in the time domain at the end of period  $z = 1000$ . The red dashed and blue solid curves correspond to  $|\psi(t, z)|$  as obtained by the numerical simulation of Eq. (3.23) and Eq. (3.24) and its theoretical prediction. (b) The soliton patterns in the frequency domain at the distance  $z = 1000$ . The red circles and blue diamonds represent  $|\hat{\psi}(\omega, z)|$  and its theoretical prediction. (c) The  $z$  dependence of  $\hat{g}(\beta(z))$  in Eq (3.24). (d) The  $z$  dependence of the soliton amplitude. The red circles and blue solid curve represent the soliton amplitude  $\eta(z)$  measured by Eqs. (3.23) and (3.24) and its theoretical prediction measured by Eqs. (3.45) and (3.46).

and compare with its theoretical prediction. The numerical simulation is implemented with Eq. (3.48) and the frequency shifting procedure for a single soliton described as in section 2.2.1. We consider **setup 5** with parameters as follows:  $\epsilon_3 = 0.01$ ,  $\beta_1(0) = 0$ ,  $\beta_2(0) = 20$ ,  $y_1(0) = 0$ ,  $y_2(0) = -20$ ,  $\eta_1(0) = \eta_2(0) = 1$ ,  $\alpha_1(0) = \alpha_2(0) = 0$ ,  $\Delta z = 0.001$ ,  $\Delta t = 0.0588$ ,  $t_{\max} = 1500$ ,  $t_{\min} = -t_{\max}$ , and  $\Delta\beta = 20$ . The numerical simulation results are presented in Fig. 10 and Fig. 11. Figure 10 illustrates the method and shows pulse patterns for repeated two-soliton collisions. Figure 11(a) depicts the amplitude dynamics  $\eta_1(z)$  with  $z_f = 5$ . We perform 5 times of the frequency shifting at the distances  $z_{s_k} = k$ , where  $k = 1, 2, \dots, 5$ . There are 5 soliton collisions at the distances  $z_{c_k} = 0.5k$ , where  $k = 1, 2, \dots, 5$ . We can see the amplitudes drop clearly after each collision as in Fig. 11(a). We have the very good agreement between the amplitude  $\eta_1(z)$  obtained by the simulation and its theoretical prediction measured from Eq. (3.57) and Eq. (3.63). Figure 11(b) presents the  $z$  dependence of the total of collision-induced amplitude shift  $\Delta\eta_1^{(c)}$ . We observe that the agreement between  $\Delta\eta_1^{(c)}$  measured by the numerical calculation with Eq. (3.67) and the theoretical calculation with Eq. (3.62) is very good. The numerical value of the accumulative collision-induced amplitude shift in 5 collisions is  $\Delta\eta_1^{(c)(num)} = -0.0093$ . The relative error, which is defined by



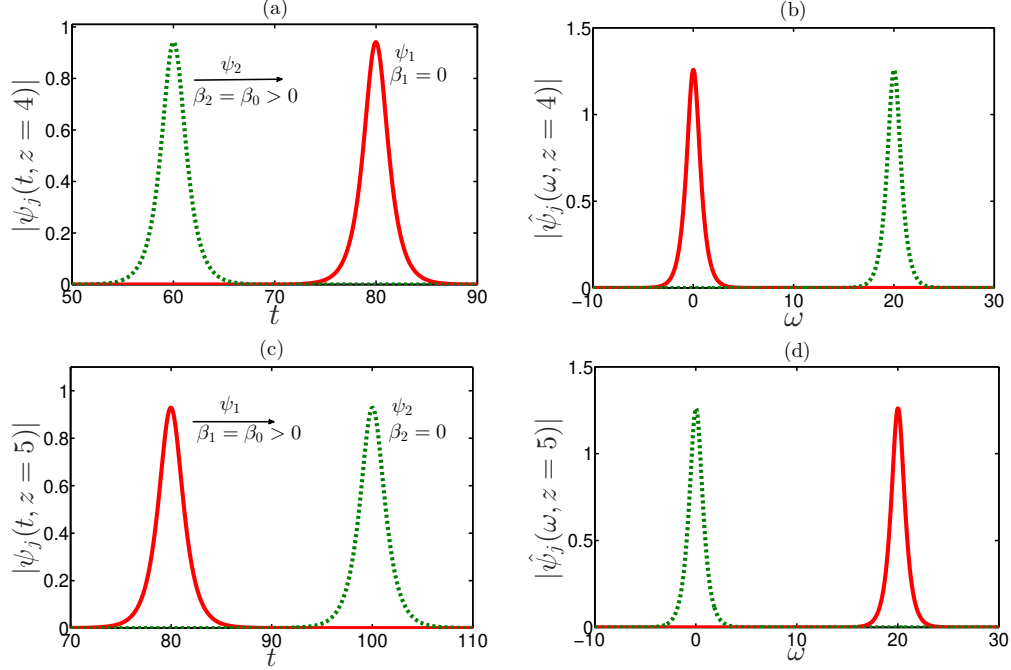


FIGURE 10. (Color online) Repeated two-soliton collisions in waveguides with weak cubic loss with Eq. (3.48) for 5 shifts of the frequency and 5 collisions with the final propagation distance  $z_f = 5$ . (a) The soliton patterns in the time domain at the distance  $z = 4$  (before the 5<sup>th</sup> collision). The red solid and green dashed curves correspond to  $|\psi_j(t, z)|$ , where  $j = 1, 2$ . (b) The soliton patterns in the frequency domain at the distance  $z = 4$ . The red solid and green dashed curves represent  $|\hat{\psi}_j(\omega, z)|$ . (c) The pulse patterns in the time domain at the final propagation distance  $z_f = 5$  (after the 5<sup>th</sup> collision). The red solid and green dashed curves are the same as in (a). (d) The soliton patterns in the frequency domain at the distance  $z = 5$ . The red solid and green dashed curves are the same as in (b).

$|\Delta\eta_1^{(c)(num)} - \Delta\eta_1^{(c)(th)}| \times 100/|\Delta\eta_1^{(c)(th)}|$ , is 0.57%. Moreover, we also implement the numerical simulations for repeating soliton collisions with 70 times of frequency shifting at distances  $z = k$  and 70 collisions at distances  $z = 0.5k$ , where  $k = 1, 2, \dots, 70$ . We measure the accumulative collision-induced amplitude shift  $\Delta\eta_1^{(c)(num)} = -0.0734$  with its relative error 0.67%. The small relative errors above confirm the robustness of the theoretical procedure for the frequency shifting and the theoretical analysis for repeating two-soliton collisions in the presence of weak cubic loss.

## 5. CONCLUSIONS

In summary, we developed the theoretical procedures of frequency shifting for solitons of the cubic NLS equation and verified them by numerical simulations. The procedures are based on simple transformations of the FT of solitons and on the shape-preserving property of solitons. The frequency shifting procedure for a single soliton is based on shifting the FT of the soliton pattern in the frequency domain. The frequency shifting procedure for a sequence of solitons is based on *the decomposition method*. In this method, we decomposed  $\Delta\beta = \Delta\beta_1 + \Delta\beta_2$ , where  $\Delta\beta_1 = 2m\pi/T$ ,  $m \in \mathbb{Z}$ , and  $-2\pi/T < \Delta\beta_2 < 2\pi/T$ , and then we implemented independently the frequency shifting for each  $\Delta\beta_j$ ,  $j = 1, 2$ , by using the different techniques for each one. To the best of our knowledge,

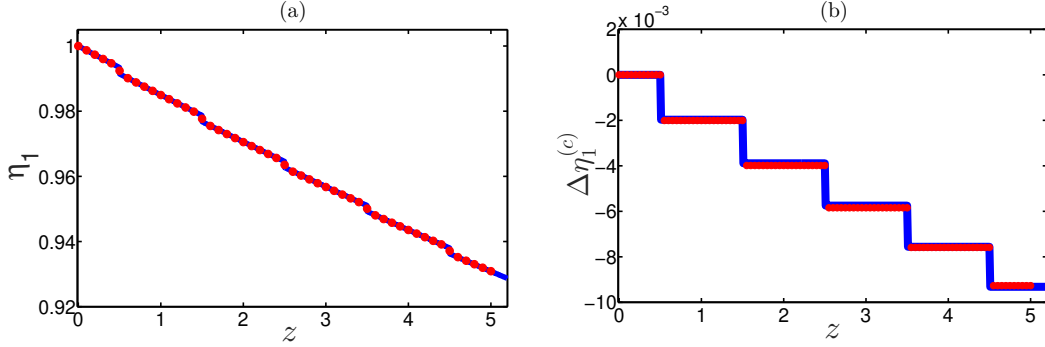


FIGURE 11. (Color online) (a) The  $z$  dependence of the soliton amplitude. The red circles and blue solid curve represent the amplitude  $\eta_1(z)$  measured by the numerical simulation with Eq. (3.48) and the theoretical amplitude  $\eta_1(z)$  obtained by Eq. (3.57) and Eq. (3.63). (b) The  $z$  dependence of the total of the collision-induced amplitude shift  $\Delta\eta_1^{(c)}$ . The red circles and blue solid curve represent the total of the collision-induced amplitude shift  $\Delta\eta_1^{(z_c)}$  measured by the numerical calculation with Eq. (3.67) and the theoretical calculation with Eq. (3.62).

the mathematical procedure of frequency shifting for a sequence of solitons by an arbitrary value has been successfully implemented and numerically verified for the first time in the current paper.

We theoretically demonstrated the use of frequency shifting procedures in two important applications: (1) stabilization of the soliton propagation in waveguides with frequency dependent linear gain-loss; (2) induction of repeated soliton collisions in waveguides with cubic loss. We showed that the amplitude dynamics of solitons in waveguides with frequency dependent linear gain-loss is described by an ODE in transmissions of a single soliton and a sequence of solitons. We used this ODE to study the robust propagation of solitons experiencing the linear loss before each frequency shifting and experiencing the linear gain after each frequency shifting. The soliton dynamics studied in this paper can be useful for controlling and guiding solitons, for example, for switching soliton dynamics (see [22, 28] for another approach to stabilize and switch sequences of solitons by using hybrid waveguides). Moreover, we demonstrated the use of the frequency shifting to enable repeated two-soliton collisions in the presence of weak cubic loss. We measured the theoretical prediction for the accumulative collision-induced amplitude shift. Our theoretical procedures and calculations are confirmed by numerical simulations with the cubic NLS equation by the split-step Fourier method. Based on the results of our numerical simulations, we conclude that the frequency procedures developed in the current paper can indeed be successfully implemented to realize stable soliton propagations and control of fast soliton collisions in nonlinear optical waveguides.

#### ACKNOWLEDGEMENTS

This work is funded by the Vietnam National Foundation for Science and Technology Development (NAFOSTED) under Grant No. 101.99-2015.29.

#### APPENDIX A. IMPLEMENTATIONS OF FREQUENCY SHIFTING FOR A SINGLE SOLITON IN NUMERICAL SIMULATIONS

Let us describe implementations of the frequency shifting in numerical simulations for the propagation of a single NLS soliton. We assume that the soliton propagation is described by Eq. (2.1) with additional weak perturbation terms. We emphasize that a similar procedure can be implemented with data obtained from experiments.

We denote by  $\psi_1^{(num)}(t, z)$  the envelope of the electric field at the propagation distance  $z$ , obtained in the simulation (or in the experiment), and by  $\hat{\psi}_1^{(num)}(\omega, z)$  the FT of  $\psi_1^{(num)}(t, z)$  with respect to time. The first step in the implementation of the frequency shifting procedure is to determine  $\Delta\beta^{(num)}$ , which is the actual value of the frequency shift to be used in the numerical simulation (or in the experiment). We determine the value of  $\Delta\beta^{(num)}$  by using:  $\Delta\beta^{(num)} = n\Delta\omega$ , where  $\Delta\omega$  is the spacing of the frequency grid in the simulation and  $n$  is the integer, whose value is closest to  $\Delta\beta/\Delta\omega$ . The *new* (frequency shifted) FT of the envelope of the electric field,  $\hat{\psi}_{1,n}^{(num)}(\omega, z)$ , is then obtained by:

$$\hat{\psi}_{1,n}^{(num)}(\omega, z) = \hat{\psi}_1^{(num)}(\omega - \Delta\beta^{(num)}, z). \quad (1.68)$$

That is,  $\hat{\psi}_{1,n}^{(num)}(\omega, z)$  is obtained by shifting  $\hat{\psi}_1^{(num)}(\omega, z)$   $n$  grid points to the right if  $\Delta\beta^{(num)} > 0$ , and  $n$  grid points to the left if  $\Delta\beta^{(num)} < 0$ . The new field  $\psi_{1,n}^{(num)}(t, z)$  is obtained by taking the inverse FT of  $\hat{\psi}_{1,n}^{(num)}(\omega, z)$  with respect to  $\omega$ .

In summary, the implementations of the frequency shifting procedure for a single soliton in simulations can be summarized by 3 steps:

- (1) Determine  $\Delta\beta^{(num)}$ .
- (2) Determine  $\hat{\psi}_{1,n}^{(num)}(\omega, z)$  by Eq. (1.68).
- (3) Determine  $\psi_{1,n}^{(num)}(t, z)$  by  $\psi_{1,n}^{(num)}(t, z) = \mathcal{F}^{-1}(\hat{\psi}_{1,n}^{(num)}(\omega, z))$ .

*Discussion.* In implementing the frequency shifting procedure for a single soliton, one needs to take care of possible consequences of the finite size of the frequency interval  $[\omega_{\min}, \omega_{\max}]$ . More specifically, suppose we employ steps (1) and (2) with  $\Delta\beta^{(num)} > 0$ . Then the values of  $\hat{\psi}_{1,n}^{(num)}(\omega, z)$  are missing at  $n$  grid points in the interval  $[\omega_{\min}, \omega_{\min} + \Delta\beta^{(num)})$  after employing the frequency shifting to the right on the frequency domain. Therefore, the values of  $\hat{\psi}_{1,n}^{(num)}(\omega, z)$  on the left tail of the pattern, i.e. for  $\omega \in [\omega_{\min}, \omega_{\min} + \Delta\beta^{(num)})$ , are determined by the extrapolation. We carry out this extrapolation by fitting  $\hat{\psi}_{1,n}^{(num)}(\omega, z)$  to the soliton part of the theoretical solution, given by Eq. (2.15), with parameters measured from the numerical simulations. That is, for  $\omega \in [\omega_{\min}, \omega_{\min} + \Delta\beta^{(num)})$ , we fit  $\hat{\psi}_{1,n}^{(num)}(\omega, z)$  to

$$\hat{\psi}_{1,n}^{(th)}(\omega, z) = \left(\frac{\pi}{2}\right)^{1/2} \frac{\exp[i\theta_n^{(num)}(z) - i\omega y^{(num)}(z)]}{\cosh\left\{\pi\left[\omega - \beta_n^{(num)}(z)\right] / [2\eta^{(num)}(z)]\right\}}, \quad (1.69)$$

where  $\eta^{(num)}(z)$ ,  $\beta_n^{(num)}(z)$ ,  $y^{(num)}(z)$ , and  $\theta_n^{(num)}(z)$  are the values of the soliton's amplitude, new frequency, position, and new overall phase, which are determined from the numerical simulation. The values of  $\hat{\psi}_{1,n}^{(num)}(\omega, z)$  on  $[\omega_{\min}, \omega_{\min} + \Delta\beta^{(num)})$  are then determined by extrapolating:  $\hat{\psi}_{1,n}^{(num)}(\omega, z) = \hat{\psi}_{1,n}^{(th)}(\omega, z)$ . Note that in a typical situation, the main body of  $\hat{\psi}_{1,n}^{(num)}(\omega, z)$  is located at the central frequency  $\beta_n^{(num)}$  and are exponentially small for  $\omega \in [\omega_{\min}, \omega_{\min} + \Delta\beta^{(num)})$ . Therefore, this extrapolation does not affect on the main body of the new soliton pattern.

## APPENDIX B. IMPLEMENTATIONS OF FREQUENCY SHIFTING FOR A SEQUENCE OF SOLITONS IN NUMERICAL SIMULATIONS

We denote by  $\psi_{sq}^{(num)}(t, z)$  the envelope of the electric field at the distance  $z$ , obtained in the simulation (or in the experiment), and by  $\hat{\psi}_{sq}^{(num)}(\omega, z)$  the FT of  $\psi_{sq}^{(num)}(t, z)$  with respect to time.

*Procedure I - a naive frequency shifting procedure.* This procedure is similar to the frequency shifting procedure for a single soliton.

*Procedure II - the frequency shifting of  $V(\omega, z)$  and  $U(\omega, z)$ .*

We first numerically measure the envelope function  $V^{(num)}(\omega, z)$  and the fast oscillation function  $W^{(num)}(\omega)$ . For this purpose, we need to measure  $\theta^{(num)}(z)$ ,  $\beta^{(num)}(z)$ ,  $\eta^{(num)}(z)$ ,  $y^{(num)}(z)$ , and  $U^{(num)}(\omega, z)$  from  $\hat{\psi}_{sq}^{(num)}(\omega, z)$ , where  $\theta^{(num)}(z)$  can be measured by  $\arg[\hat{\psi}_{sq}^{(num)}(0, z)]$  and  $U^{(num)}(\omega, z) = \theta^{(num)}(z) - \omega y^{(num)}(z)$ . We then measure the normalized envelope function:

$$V^{(num)}(\omega, z) = \tilde{V}^{(num)}(\omega, z)/(2J + 1), \quad (2.70)$$

where the envelope function  $\tilde{V}^{(num)}(\omega, z)$  is tangential to  $|\hat{\psi}_{sq}^{(num)}(\omega, z)|$ . The function  $\tilde{V}^{(num)}(\omega, z)$  can be measured by collecting the coordinates of all the points on the graph of the numerical  $|\hat{\psi}_{sq}^{(num)}(\omega, z)|$  where the curve of  $|\hat{\psi}_{sq}^{(num)}(\omega, z)|$  is tangential to the function bounding  $|\hat{\psi}_{sq}^{(num)}(\omega, z)|$  from above. Once all these coordinates were collected, we also need to carry out an interpolation at other  $\omega$ -values by using Eq. (2.12) as follows:

$$V^{(th)}(\omega, z) = (\pi/2)^{1/2} \operatorname{sech} \left\{ \pi \left[ \omega - \beta^{(num)}(z) \right] / \left[ 2\eta^{(num)}(z) \right] \right\}. \quad (2.71)$$

After measuring  $V^{(num)}(\omega, z)$ , we measure the fast oscillating function  $W^{(num)}(\omega)$  by

$$W^{(num)}(\omega) = \hat{\psi}_{sq}^{(num)}(\omega, z) e^{-iU^{(num)}(\omega, z)} / V^{(num)}(\omega, z). \quad (2.72)$$

We note that  $V^{(num)}(\omega, z)$  is exponentially approaching to 0 on both tails in the frequency domain. Therefore, the division in Eq. (2.72) can be numerically invalid when  $V^{(num)}(\omega, z)$  is small enough. Let  $L$  be length of the interval centered at  $\beta^{(num)}(z)$  such that the division in Eq. (2.72) can be numerically valid, i.e., the division is implemented accurately with small relative errors. Based on extensively numerical tests with different values of  $L$ , we find that the typical values of  $L$  is  $15 \leq L \leq 40$ . Thus, Eq. (2.72) can be invalid for  $\omega < \beta^{(num)}(z) - L/2$  or  $\omega > \beta^{(num)}(z) + L/2$ . We therefore need to implement the extrapolation of  $W^{(num)}(\omega)$  to its theoretical function  $W^{(th)}(\omega)$  by using Eq. (2.13) for  $\omega < \beta^{(num)}(z) - L/2$  or  $\omega > \beta^{(num)}(z) + L/2$ .

Second, we implement the following transformations:  $V_n^{(num)}(\omega, z) = V^{(num)}(\omega - \Delta\beta^{(num)}, z)$  and  $U_n^{(num)}(\omega, z) = U^{(num)}(\omega - \Delta\beta^{(num)}, z)$ , where  $\Delta\beta^{(num)}$  is the actually numerical frequency shift value. Note that we need the theoretical predictions  $V_n^{(th)}(\omega, z)$  defined by

$$V_n^{(th)}(\omega, z) = (\pi/2)^{1/2} \operatorname{sech} \left\{ \pi \left[ \omega - \beta_n^{(num)}(z) \right] / \left[ 2\eta^{(num)}(z) \right] \right\} \quad (2.73)$$

and  $U_n^{(th)}(\omega, z) = \theta_n^{(num)}(z) - \omega y^{(num)}(z)$  to extrapolate the missing data of  $V_n^{(num)}(\omega, z)$  and  $U_n^{(num)}(\omega, z)$  when employing the transformation  $\omega \rightarrow \omega - \Delta\beta^{(num)}$ . Here,  $\beta_n^{(num)}(z) = \beta^{(num)}(z) + \Delta\beta^{(num)}$  and  $\theta_n^{(num)}(z) = \theta^{(num)}(z) + \Delta\beta^{(num)} y^{(num)}(z)$ .

Third, we define the new sequence of solitons in the frequency domain by

$$\hat{\psi}_{sq,n}^{(num)}(\omega, z) = V_n^{(num)}(\omega, z) W^{(num)}(\omega) e^{iU_n^{(num)}(\omega, z)}. \quad (2.74)$$

Finally, we take the inverse FT of  $\hat{\psi}_{sq,n}^{(num)}(\omega, z)$  with respect to  $\omega$  to obtain  $\psi_{sq,n}^{(num)}(t, z)$  with the new frequency of  $\beta(z) + \Delta\beta^{(num)}$  as desired.

*Procedure III - the decomposition procedure.*

First, we decompose  $\Delta\beta^{(num)}$ :  $\Delta\beta^{(num)} = \Delta\beta_1 + \Delta\beta_2$ , where  $\Delta\beta_1 = 2m\pi/T$  with  $m$  is the nearest integer rounded by  $\Delta\beta^{(num)}T/2\pi$  and  $-2\pi/T < \Delta\beta_2 < 2\pi/T$ .

Second, we shift the frequency of  $\hat{\psi}_{sq}^{(num)}(\omega, z)$  by  $\Delta\beta_1$  with the transformation  $\omega \rightarrow \omega - \Delta\beta_1$  as in *procedure I*:

$$\hat{\psi}_{sq,n1}^{(num)}(\omega, z) = \hat{\psi}_{sq}^{(num)}(\omega - \Delta\beta_1, z). \quad (2.75)$$

Note that we also need to extrapolate the missing data of  $\hat{\psi}_{sq,n1}^{(num)}$  by its theoretical prediction  $\hat{\psi}_{sq,n1}^{(th)}$  when implementing the transformation  $\omega \rightarrow \omega - \Delta\beta_1$  similar to implement the frequency shifting for a single soliton.

Third, we implement the frequency shifting of the value  $\Delta\beta_2$  for  $\hat{\psi}_{sq,n1}^{(num)}(\omega, z)$  with the *procedure II*. We need to measured functions  $V^{(num)}(\omega, z)$  and  $W^{(num)}(\omega)$  of  $\hat{\psi}_{sq,n1}^{(num)}(\omega, z)$ . We then employ the transformations:  $V_n^{(num)}(\omega, z) = V^{(num)}(\omega - \Delta\beta_2, z)$  and  $U_n^{(num)}(\omega, z) = U^{(num)}(\omega - \Delta\beta_2, z)$ . The extrapolation for  $V_n^{(num)}(\omega, z)$  and  $U_n^{(num)}(\omega, z)$  is also implemented in this step as in the *procedure II*.

Fourth, we define the new sequence of solitons in the frequency domain by

$$\hat{\psi}_{sq,n}^{(num)}(\omega, z) = V_n^{(num)}(\omega, z)W^{(num)}(\omega)e^{iU_n^{(num)}(\omega, z)}. \quad (2.76)$$

Finally, we take the inverse FT of  $\hat{\psi}_{sq,n}^{(num)}(\omega, z)$  with respect to  $\omega$  to obtain  $\psi_{sq,n}^{(num)}(t, z)$ .

In summary, the implementations for the decomposition procedure include 5 main steps:

- (1) Decompose  $\Delta\beta^{(num)} = \Delta\beta_1 + \Delta\beta_2$ , where  $\Delta\beta_1 = 2m\pi/T$  and  $-2\pi/T < \Delta\beta_2 < 2\pi/T$ .
- (2) Define  $\hat{\psi}_{sq,n1}^{(num)}(\omega, z)$  by the *procedure I* with  $\Delta\beta_1$  and Eq. (2.75).
- (3) Measure  $V^{(num)}(\omega, z)$  and  $W^{(num)}(\omega)$  of  $\hat{\psi}_{sq,n1}^{(num)}(\omega, z)$ .
- (4) Define  $\hat{\psi}_{sq,n}^{(num)}(\omega, z)$  by the *procedure II* with  $\Delta\beta_2$  and Eq. (2.76).
- (5) Compute  $\psi_{sq,n}^{(num)}(t, z) = \mathcal{F}^{-1}(\hat{\psi}_{sq,n}^{(num)}(\omega, z))$ .

## APPENDIX C. SPLIT-STEP FOURIER METHOD

One method that has been used extensively to solve the pulse-propagation problem in nonlinear dispersive media is the split-step Fourier method, which is a pseudo-spectral method. In this Appendix, we briefly describe the split-step Fourier method to implement the numerical simulations of the perturbed NLS equation [6, 33, 38]. We re-write the perturbed NLS equation in the form:

$$\partial_z \psi = (L + N)\psi, \quad (3.77)$$

where  $L$  is the linear and  $N$  is the nonlinear operator. For example, if we solve the NLS with weak cubic loss:  $i\partial_z \psi + \partial_t^2 \psi + 2|\psi|^2 \psi = -i\epsilon_3 |\psi|^2 \psi$ , then  $L\psi = i\partial_t^2 \psi$ , and  $N\psi = (2i - \epsilon_3)|\psi|^2 \psi$ . The theoretical exact solution of Eq. (3.77) at the propagation distance  $z + h$  can be written as

$$\psi(z + h, t) = \exp[h(L + N)]\psi(z, t), \quad (3.78)$$

where  $h = \Delta z$  is a small propagation distance for the propagation of soliton from  $z$  to  $z + h$  in optical waveguide ( $h$  is a  $z$ -step size).

In general, dispersion and nonlinearity act together along the length of the waveguide. In the split-step Fourier method, we assume that the linear and nonlinear effects act independently in the propagation of solitons over a small distance  $h$ . The propagation from  $z$  to  $z + h$  is carried out in two steps. In the first step, the nonlinearity acts alone and in the second step, dispersion acts alone. We thus consider two split equations:

$$\partial_z \psi = L\psi, \quad (3.79)$$

and

$$\partial_z \psi = N\psi. \quad (3.80)$$

The solution at the propagation distance  $z + h$  of Eq. (3.79) and Eq. (3.80) can be written as  $e^{hL}\psi(z, t)$  and  $e^{hN}\psi(z, t)$ , respectively. Using the Baker-Hausdorff formula for two non-commutative

operators  $A, B$  where  $A = hL, B = hN$ :

$$\exp(A) \exp(B) = \exp\left(A + B + \frac{1}{2}[A, B] + \frac{1}{12}[A - B, [A, B]] + \dots\right), \quad (3.81)$$

the error  $E = |\exp(h(L + N)) - \exp(hL) \exp(hN)|$  is found to result from  $\frac{1}{2}h^2 [N, L]$ , i.e, in the second order. The error can be reduced to the order  $o(h^n)$  if we can find a set of real numbers  $(c_l, c_2, \dots, c_n)$  and  $(d_l, d_2, \dots, d_n)$  such that

$$\exp(h(L + N)) = \prod_{i=1}^n \exp(c_i hL) \exp(d_i hN) + o(h^{n+1}). \quad (3.82)$$

Using the results in [37], one can obtain:

$$\begin{aligned} c_1 &= \frac{1}{2(2 - 2^{1/3})}, c_2 = \frac{1 - 2^{1/3}}{2(2 - 2^{1/3})}, c_3 = c_2, c_4 = c_1, \\ d_1 &= \frac{1}{(2 - 2^{1/3})}, d_2 = \frac{-2^{1/3}}{(2 - 2^{1/3})}, d_3 = d_1, d_4 = 0. \end{aligned} \quad (3.83)$$

The split-step expressions in Eqs. (3.82)-(3.83) are fourth-order accurate [33, 37]. The linear part  $e^{c_i hL}$  can be numerically calculated by using the fast FT (FFT) [32]. Note that using definition to compute a discrete FT of  $n$  points takes  $O(n^2)$  arithmetical operations, while an FFT can compute the same result in only  $O(n \ln n)$  operations. This speeds up the computation compared with most finite difference schemes [6, 32]. The nonlinear part  $e^{d_i hN}$  can be solved by using Runge-Kutta fourth-order method. A sufficient condition for numerical stability is  $\frac{\Delta z}{\Delta t^2} < \frac{1}{\pi}$  [33, 39].

## REFERENCES

- [1] A.C. Newell, *Solitons in Mathematics and Physics*, SIAM, Philadelphia, 1985.
- [2] T. Tao, *Why are solitons stable?*, Bull. Amer. Math. Soc. **46** (2009), 1-33.
- [3] T. Tao, *Nonlinear Dispersive Equations: Local and Global Analysis*, CBMS Regional Conference Series in Mathematics **106** 2006, AMS.
- [4] S. Novikov, S.V. Manakov, L.P. Pitaevskii, and V.E. Zakharov, *Theory of Solitons: The Inverse Scattering Method*, Plenum, New York, 1984.
- [5] Y.S. Kivshar and B.A. Malomed, *Dynamics of solitons in nearly integrable systems*, Rev. Mod. Phys. **61** (1989), 763.
- [6] G.P. Agrawal, *Nonlinear Fiber Optics*, Academic, San Diego, CA, 2001.
- [7] J.N. Kutz, *Mode-Locked Soliton Lasers*, SIAM Rev. **48** (2006), 629-679.
- [8] L.F. Mollenauer and J.P. Gordon, *Solitons in Optical Fibers: Fundamentals and Applications*, Academic, San Diego, CA, 2006.
- [9] W. Horton and Y.H. Ichikawa, *Chaos and Structure in Nonlinear Plasmas*, World Scientific, Singapore, 1996.
- [10] N. J. Zabusky and M. D. Kruskal, *Interaction of "solitons" in a collisionless plasma and the recurrence of initial states*, Phys. Rev. Lett. **15** (1965), 240.
- [11] N. J. Zabusky, *Fermi-Pasta-Ulam, solitons and the fabric of nonlinear and computational science: History, synergetics, and visiometrics*, Chaos **15** (2005), 015102.
- [12] M.J. Ablowitz and H. Segur, *Solitons and The Inverse Scattering Transform*, SIAM, Philadelphia, 1981.
- [13] A. Hasegawa and F. Tappert, *Transmission of stationary nonlinear optical pulses in dispersive dielectric fibers. Part I. Anomalous dispersion; Part II. Normal dispersion*, Appl. Phys. Lett. **23** (1973), 142-144, 171-173.
- [14] S. J. B. Yoo, *Wavelength Conversion Technologies for WDM Network Applications*, J. Light. Technol. **14** (1996), 955-966.
- [15] E. Ip, A. P. T. Lau, D. J. F. Barros, and J. M. Kahn, *Coherent detection in optical fiber systems*, Opt. Express **16** (2008), 753.
- [16] F. M. Mitschke and L. F. Mollenauer, *Discovery of the soliton self-frequency shift*, Opt. Lett. **11** (1986), 659-661.
- [17] D.R. Burton, A.J. Goodall, J.T. Atkinson, and M.J. Lalor, *The use of carrier frequency shifting for the elimination of phase discontinuities in Fourier transform profilometry*, Opt. Lasers Eng. **23** (1995), 245-257.
- [18] D. V. Skryabin, F. Luan, J.C. Knight, and P.S. Russell, *Soliton self-frequency shift cancellation in photonic crystal fibers*, Science **301** (2003), 1705-1708.



- [19] Y. Chung and A. Peleg, *Strongly non-Gaussian statistics of optical soliton parameters due to collisions in the presence of delayed Raman response*, Nonlinearity **18** (2005), 1555-1574.
- [20] A. Peleg and D. Chakraborty, *Enhancement of transmission quality in soliton-based optical waveguide systems by frequency dependent linear gain-loss and the Raman self-frequency shift*, arXiv:1804.03226 (2018).
- [21] D. Chakraborty, A. Peleg, and Q. M. Nguyen, *Stabilizing soliton-based multichannel transmission with frequency dependent linear gain-loss*, Opt. Commun. **371** (2016) 252-262.
- [22] A. Peleg, Q.M. Nguyen, and T.T. Huynh, *Stable scalable control of soliton propagation in broadband nonlinear optical waveguides*, Eur. Phys. J. D **71** (2017), 30.
- [23] A. Peleg and D. Chakraborty, *Large stable oscillations due to Hopf bifurcations in amplitude dynamics of colliding soliton sequences*, Commun. Nonlinear Sci. Numer. Simulat. **63** (2018), 145-160.
- [24] M. A. Foster, A. C. Turner, J. E. Sharping, B. S. Schmidt, M. Lipson, and A. L. Gaeta, *Broad-band optical parametric gain on a silicon photonic chip*, Nature (London) **441** (2006), 960-963.
- [25] A. Peleg, Q.M. Nguyen, and Y. Chung, *Crosstalk dynamics of optical solitons in a broadband Kerr nonlinear system with weak cubic loss*, Phys. Rev. A **82** (2010), 053830.
- [26] Y. Okawachi, O. Kuzucu, M.A. Foster, R. Salem, A.C. Turner-Foster, A. Biberman, N. Ophir, K. Bergman, M. Lipson, and A.L. Gaeta, *Characterization of Nonlinear Optical Crosstalk in Silicon Nanowaveguides*, IEEE Photon. Technol. Lett. **24** (2012), 185.
- [27] C. Husko, S. Combr  , P. Colman, J. Zheng, A. De Rossi and C.W. Wong, *Soliton dynamics in the multiphoton plasma regime*, Sci. Rep. **3** (2013), 1100.
- [28] Q.M. Nguyen, A. Peleg, and T.P. Tran, *Robust transmission stabilization and dynamic switching in broadband hybrid waveguide systems with nonlinear gain and loss*, Phys. Rev. A **91** (2015), 013839.
- [29] The dimensionless distance  $z$  in Eqs. (2.1) and Eq. (3.23) is  $z = X/(2L_D)$ , where  $X$  is the dimensional distance,  $L_D = \tau_0^2/|\tilde{\beta}_2|$  is the dimensional dispersion length,  $\tau_0$  is the soliton width, and  $\tilde{\beta}_2$  is the second-order dispersion coefficient. The dimensionless time is  $t = \tau/\tau_0$ , where  $\tau$  is the time.  $\psi = E/\sqrt{P_0}$ , where  $E$  is proportional to the electric field and  $P_0$  is the peak power. The coefficient  $g$  is related to the linear gain-loss coefficient  $\tilde{g}$  by  $g = 2\tau_0^2\tilde{g}/|\tilde{\beta}_2|$ , respectively. The solitons spectral width is  $\nu_0 = 1/(\pi^2\tau_0)$  and the intersequence frequency difference is  $\Delta\nu = (\pi\Delta\beta\nu_0)/2$ .
- [30] R. Hirota, *Exact envelope-soliton solutions of a nonlinear wave equation*, J. Math. Phys. **14** (1973), 805.
- [31] A. Hasegawa and Y. Kodama, *Solitons in Optical Communications*, Clarendon, Oxford, 1995.
- [32] L. N. Trefethen, *Spectral Methods in MATLAB*, SIAM, Philadelphia, 2000.
- [33] J. Yang, *Nonlinear Waves in Integrable and Nonintegrable Systems*, SIAM, Philadelphia, 2010.
- [34] D.J. Kaup, *Closure of the squared Zakharov-Shabat eigenstates*, J. Math. Anal. Appl. **54** (1976), 849-864.
- [35] D.J. Kaup, *A Perturbation Expansion for the Zakharov-Shabat Inverse Scattering Transform*, SIAM J. Appl. Math. **31** (1976), 121-133.
- [36] I.S. Gradshteyn and I.M. Ryzhik, *Table of integrals, series, and products*, Academic, San Diego, CA, 2007.
- [37] H. Yoshida, *Construction of higher order symplectic integrators*, Phys. Lett. A **150** (1990), 262-268.
- [38] J. A. C. Weideman and B. M. Herbst, *Split-step methods for the solution of the nonlinear Schr  dinger equation*, SIAM J. Numer. Anal., **23** 1986, 485-507.
- [39] T.I. Lakoba, *Instability analysis of the split-step Fourier method on the background of a soliton of the nonlinear Schr  dinger equation*, Numer. Methods Partial Differ. Equ. **28** (2012), 641-669.

(T.T. Huynh) DEPARTMENT OF MATHEMATICS, UNIVERSITY OF SCIENCE, VIETNAM NATIONAL UNIVERSITY-HCMC, HO CHI MINH CITY, VIETNAM

DEPARTMENT OF MATHEMATICS, UNIVERSITY OF MEDICINE AND PHARMACY AT HO CHI MINH CITY, HO CHI MINH CITY, VIETNAM

E-mail address: huynhthanhthoan@ump.edu.vn

(Q.M. Nguyen) DEPARTMENT OF MATHEMATICS, INTERNATIONAL UNIVERSITY, VIETNAM NATIONAL UNIVERSITY-HCMC, HO CHI MINH CITY, VIETNAM

E-mail address: quannm@hcmiu.edu.vn